THE JOURNAL OF PHYSICAL CHEMISTRY B
A JOURNAL OF THE AMERICAN CHEMICAL SOCIETY

pubs.acs.org/JPCB

Article

Transfer Matrix Model of pH Effects in Polymeric Complex Coacervation

Ashley R. Knoerdel, Whitney C. Blocher McTigue, and Charles E. Sing*

Cite This: *J. Phys. Chem. B* 2021, 125, 8965–8980

Read Online

ABSTRACT: Oppositely charged polyelectrolytes can undergo an associative phase separation, in a process known as polymeric complex coacervation. This phenomenon is driven by the electrostatic attraction between polyanion and polycation species, leading to the formation of a polymer-dense coacervate phase and a coexisting polymer-dilute supernatant phase. There has been significant recent interest in the physical origin and features of coacervation; yet notably, experiments often use weak polyelectrolytes the charge state of which depends on solution pH, while theoretical or computational efforts typically assume strong polyelectrolytes that remain fully charged. There have been only a few efforts to address this limitation, and thus there has been little exploration of how pH can affect complex coacervation. In this paper, we modify a transfer matrix theory of coacervation to account for acid−base equilibria, taking advantage of its ability to directly account for some local ion correlations that will affect monomer charging. We show that coacervation can stabilize the charged state of a weak polyelectrolyte via the proximity of oppositely charged monomers, and can lead to asymmetric phase diagrams where the positively and negatively charged polyelectrolytes exhibit different behaviors near the pK_a of either chain. Specifically, there is a partitioning of one of the salt species to a coacervate to maintain electroneutrality when one of the polyelectrolytes is only partially charged. This results in the depletion of the same salt species in the supernatant, and overall can suppress phase separation. We also demonstrate that, when one of the species is only partially charged, mixtures that are off-stoichiometric in volume fraction but stoichiometric in charge exhibit the greatest propensity to form coacervate phases.

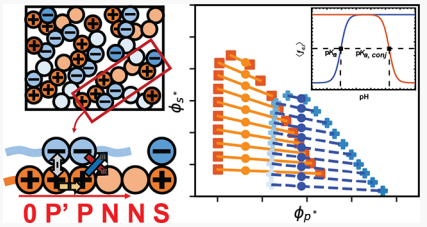

INTRODUCTION

Complex coacervation is an associative, liquid−liquid phase separation phenomenon between oppositely charged macroions[1−12] (e.g., polymers,[13−18] proteins,[19−22] surfactant micelles,[23−28] and colloids[29]) driven by electrostatic attraction between the positively and negatively charged species. The result is a dense macroion-rich phase called the coacervate and a macroion-dilute phase called the supernatant. Coacervates have found use as encapsulants, additives, emulsifiers, and viscosity modifiers in food science and personal care products.[30−35] Furthermore, their utility has extended into other fields such as adhesives,[36−48] drug delivery,[5,7−9,11,14,17,49−65] nano/bioreactors,[13,16,66−68] and cellular biology.[57,69−84] In addition, complex coacervation has been used as a strategy for protein and drug encapsulation due to the gentle sequestration coacervation provides without the use of harsh organic solvents.[5,52,85,86] This wide variety of applications is due to the ease by which coacervates can be engineered to exhibit a wide range of physical and chemical properties, by adjusting either the macroions or their environment.

Recently, there has been intense interest in predicting the relationship between coacervate properties and their molecular components or environmental parameters. This has prompted a resurgence of experimental, computational, and theoretical study into this phenomenon, with particular focus on *polymeric* complex coacervates formed from two oppositely charged polyelectrolytes. Experimental efforts have studied how these systems are affected by their environment (e.g., pH,[1,87−89] salt concentration, and identity,[1,87,90,91] and temperature[87]) and the molecular features of the polyelectrolytes themselves (e.g., polymer stiffness and charge density,[92] chirality,[3,4] molecular weight, charge sequence,[93] architecture,[94] and stoichiometry[1,87,95]). Variation of these parameters are evident in a number of observables, such as solution turbidity,[6,86] surface tension,[25] solution thermodynamics,[93] and bulk rheology.[96−99] Most of these experimental observables reflect the underlying structure and phase behavior of coacervation, which has been mapped in a number of papers that plot the two-phase coexistence region at low salt and polymer concentrations.[90,100−102] The large number of molecular and system parameters, and their corresponding physical properties, underscores why coacervation is useful in such an array of applications; yet, this same complexity is a daunting challenge for even systematic experimental studies, which struggle to span such a vast

Received: April 5, 2021
Revised: June 17, 2021
Published: July 30, 2021

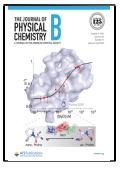

parameter space. This motivates the use of simulation and theory, in pursuit of a physical picture of coacervation consistent with experimental data.

Advances in the experimental study of coacervation has been accompanied by significant progress in computational and theoretical modeling, driven by a need to develop a more sophisticated alternative to the classical Voorn-Overbeek theory[90,103,104] that combines Flory-Huggins theory of polymer mixing[105] with a Debye-Hückel free energy of charge interactions.[106,107] Most recent efforts aim to overcome the deficiencies of this model,[100,101,108,109] which are that (1) Voorn-Overbeek theory inaccurately treats polymer charges as isolated, despite being connected along the polyelectrolyte chains and (2) Debye−Hückel itself is only accurate in the low-salt limit.[107] These deficiencies have been addressed in a number of different ways, such as more sophisticated polymer field theories,[102,110−119] scaling arguments,[120−125] and liquid state theories.[95,109,126] The advantages and disadvantages of these approaches have been discussed elsewhere,[108,127] but each has contributed to a more coherent picture of coacervation that is still being developed. Coarse-grained simulation[100,101,128−130] (and, recently, atomistic simulation)[3,131] has also played an important role in interrogating these theoretical advances, providing a molecular snapshot of coacervation that supports the existence of a dense polyelectrolyte phase that is indeed well beyond the regime governed by Debye−Hückel electrostatics.

Despite significant advances in experiment and modeling of complex coacervation, there remains practical and fundamental challenges in using these new insights to guide emerging coacervation applications such as protein and drug encapsulation. In these situations, there is a focus on using polypeptides and biopolymers because of their biocompatibility;[2,5,41,132] coacervation is inherently useful in these situations, due to its sensitivity to the electrostatic/ionic environment,[1,27,49,86,133−135] but biomolecular chemistry can be far more complicated than the model systems considered in fundamental research. Molecular features common in biomacromolecules (e.g., sequence-definition, semiflexibility, hydrophobicity) can complicate the already-challenging physical picture of coacervation. In addition to these molecular challenges, most biomacromolecules (and also many synthetic polymers) are weak polyelectrolytes that change their charge state in response to the solution pH.[1,86]

pH effects are especially important to understand in the context of coacervation, as the electrostatics that drive phase separation will be sensitive to the local environment. Experimental investigations typically circumvent the challenge of considering pH effects in one of two ways: (1) they rely on *strong* polyelectrolytes that are essentially always fully charged[96,97,136] or (2) they choose polyelectrolytes with a sufficiently large window between their respective pK_a values and carefully check to ensure that the chains form coacervates at stoichiometric ratios of charge.[4,5,132] The first strategy uses polymers such as poly(styrenesulfonate, sodium salt) (pSS), which has a pK_a of approximately 1.2−1.5 at low concentrations so it is fully charged at most reasonable pH values.[137] The second strategy is more common, however, due to the abundance of weak polyelectrolytes with a pK_a roughly between 2 and 10; these polymers will be partially dissociated at intermediate pH values, where a majority of experiments occur. Polypeptides are a prime example of weak polyelectrolytes, as are other biopolymers. For instance, the component peptides of poly(aspartate) and poly(lysine) have pK_a values of ∼3.9 and ∼10.5, respectively, which we will use in this manuscript.[138] Despite these strategies, which are useful for fundamental studies on coacervate phenomena, in many applications it is common for polyelectrolytes to be near their pK_a during complexation. This is especially true in situations in which the environment pH is less than 2 pH units away from the pK_a of one of the polyelectrolytes, where the polyelectrolyte in question is assumed to be less than fully charged.[4,132,139] Perry et al. conducted experiments between poly(acrylic acid, sodium salt) (pAA) and poly(allylamine hydrochloride) (pAH) that had pK_a values of 4.5 and 8.5, respectively, at both pH 6.5 and 8.5.[1] At pH 8.5, pAH is only half charged due to the pH being equivalent to the pK_a, thus assuming fully charged polymers would no longer represent the system. Tekaat and co-workers also utilized pAA with a strong polyelectrolyte at a wide range of pH values (5 to 10) to evaluate the time-pH superpositon of these complex coacervates.[98] Similar to Perry et al., Tekaat et al. utilized situations where pAA was not fully charged as the pH of the system was near to the pK_a.

There have been only a few theoretical or computational efforts to understand pH effects in coacervation.[88,140−142] This is in part due to the challenge of modeling acid−base equilibria in polyelectrolytes, which is complicated by the correlated charge environment around participating monomers.[143−147] Unlike small molecule acids and bases, monomers are typically closely connected to adjacent monomers that can also be charged and suppress dissociation. This insight has formed the foundation of theoretical approaches to weak polyelectrolyte systems, where acid−base equilibria can be incorporated into a system semigrand free energy via a reservoir chemical potential of the participating species.[143] The external reservoir pH is thus the controlled parameter, with charge confinement and electrostatic attraction affecting both the dissociated fraction and local pH in ways that are distinct from the small-molecule limit.[143,145] This results in a shift of the *effective* pK_a (p$K_{a,eff}$, i.e., where the fraction of dissociated monomers $f = 0.5$) that stabilizes the uncharged state, an effect that can be exacerbated in a number of confined polyelectrolyte systems such as brushes or gels.[143−147] Recently, simulations have demonstrated that polyelectrolyte complexation exhibits the opposite trend; in simulations of two complexing polyectrolytes, the strong electrostatic attraction between the chains promotes charging, in contrast to the electrostatic repulsion between adjacent monomers.[88,140] Only a few papers have incorporated pH effects into the modeling of bulk coacervates; Larson and co-workers have incorporated this via equilibrium constants in their coacervate model, as one of a few competing "effective" reactions that also includes the ion pairing interactions that play an important role in coacervation.[141,142]

In this paper, we expand on our recent "transfer matrix" model of coacervation to account for pH effects.[129,130,148−150] This model is similar to the Larson model[141,142,151] in that it attempts to account for ion pairing effects in coacervates, but in this case does so by mapping the entire set of ion pairing interactions to an adsorption model. A test polyelectrolyte chain serves as an adsorption substrate, upon which "paired" oppositely charged species are adsorbed. This approach is motivated by the importance of neighboring charges in the polymer−polymer and polymer−salt correlations observed in molecular simulations,[100] and has demonstrated success in modeling a wide range of coacervate phenomena.[129,130,148−150] This model demonstrates excellent matching with simulation (both in terms of phase behavior and molecular structure),[148] and can be modified to

https://doi.org/10.1021/acs.jpcb.1c03065
J. Phys. Chem. B 2021, 125, 8965−8980

capture effects such as chain stiffness,[149] multivalent charges,[149] charge monomer sequence,[130,150] coacervate interfaces,[129] and block copolyelectrolyte self-assembly.[152] It also serves as a natural way of incorporating pH effects, due to the explicit treatment of interactions between neighboring monomers along the same polyelectrolyte chain. We show that, with straightforward arguments for these interactions, we can recapitulate the shifts in $pK_{a,eff}$ expected for both isolated and complexed polyelectrolytes,[141,153] and show how this affects the phase behavior of coacervates formed from these systems. We show this phase behavior in a number of ways, both in terms of experimentally relevant quantities as well as diagrams that plot the concentrations of all five components. At most intermediate pH values, the system behaves nearly identical to that of a strong polyelectrolyte coacervate, but near the $pK_{a,eff}$ the phase behavior can become significantly asymmetric with respect to the positively and negatively charged species.

MODEL AND COMPUTATIONAL METHODS

In this paper, we model weak polyelectrolyte coacervates using the transfer matrix approach, which accounts for local charge correlations in polyelectrolyte solutions by enumerating species that are spatially adjacent due to either "ion pairing" or polymer connectivity.[148] We justified this approach by observing that the features of pair correlation functions in simulation models are primarily governed by immediately adjacent neighbors, with longer-range correlations such as those predicted by Debye-Hückel or Poisson-Boltzmann arguments almost completely absent at the high salt and polymer concentrations relevant for coacervation.[100,129] Our theory keeps track of these neighboring charges by mapping the complicated, three-dimensional structure of a coacervate (see schematic in Figure 1a) to a one-dimensional adsorption model; a test polyelectrolyte chain is treated as a series of adsorption sites, onto which oppositely charged species can adsorb. Each site can then be in any one of five different states, illustrated in Figure 1b; if the site is itself charged, it can be paired with the oppositely charged salt (S), the oppositely charged polyelectrolyte (P or P′), or can remain unpaired (0). In this paper, we introduce the possibility that the site can be uncharged (N), as controlled by the acid−base equilibria and pH of the solution. For a charged site that is bound to a polymer, we further distinguish an initially bound polyelectrolyte charge (P′) and any subsequent charges (P) that belong to the same bound chain.

We first write a grand canonical partition function for this adsorption model, which summates over the various microstates $\{s_i\}$ that are defined by the states s_i = (S, P, P′, 0, N) associated with all adsorption sites i (i.e., the monomers along the test chain):

$$\Xi_{int,+} = \sum_{\{s_i\}}{}' \exp[-\beta \Delta W_+(\{s_i\})] \tag{1}$$

The apostrophe on the summation indicates the constraint that P must follow either a P′ or P, and we consider a test polycation as an example. The grand potential $\Delta W_+ = W_+(\{s_i\}) - W_{ref,+}$ accounts for all of the direct Coulomb interactions, along with the chemical potentials associated with the adsorbing species and reference chemical potentials for the acid−base equilibrium reactions. These are incorporated into the $W_+(\{s_i\})$ term:

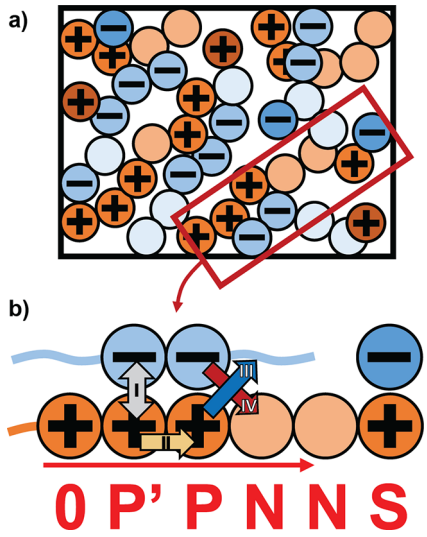

Figure 1. (a) Schematic illustrating a coacervate-forming polyelectrolyte solution, consisting of weakly charged polycations (orange) with both charged and uncharged monomers, and weakly charged polyanions (blue) with both charged and uncharged monomers. Cations and anions are shown in dark orange and blue, respectively. Test polymers, such as the boxed polycation, can be mapped to an adsorption model as in panel b, with adsorption states denoted as S, P, P′, 0, or N. In this model, we consider contributions to the electrostatic energy from adjacent and nearly adjacent charged species. This includes adsorbed oppositely charged species (i), neighboring like-charged monomers (ii), and interactions with oppositely charged species on neighboring sites (iii) and (iv).

$$\begin{aligned}\beta W_+(\{s_i\}) = \sum_{i=1}^{N-1} \Big\{ & \Gamma_0[(1-\delta_{s_i,N})(1-\delta_{s_{i+1},N}) - (1-\delta_{s_{i+1},N}-\delta_{s_{i+1},0})] \\ & - \Gamma_1[(1-\delta_{s_i,N})(1-\delta_{s_{i+1},N}-\delta_{s_{i+1},0}) + (1-\delta_{s_i,N}-\delta_{s_i,0}) \\ & (1-\delta_{s_{i+1},N})] - \delta_{s_i,P}\delta_{s_{i+1},P}\ln(E) - \delta_{s_i,P}\delta_{s_{i+1},P}\ln(2E)\Big\} \\ & - \sum_{i=0}^{N-1}\Big\{\delta_{s_{i+1},P}\beta\mu_{P-} + \delta_{s_{i+1},S}\beta\mu_{S-} + (1-\delta_{s_{i+1},N})\beta\mu^0_{P+} \\ & + \delta_{s_{i+1},N}\beta\mu^0_{POH}\Big\}\end{aligned} \tag{2}$$

In this form of the interaction term, we introduce a Kronecker delta $\delta_{s_i,X}$, which is zero unless the state s_i of monomer i is X. Each term in the first summation considers the monomer i and its next monomer $i + 1$, accounting for interactions between adjacent monomers, while the second summation considers only the next monomer $i + 1$. The first term accounts for the pairwise like-charge repulsions between adjacent monomers (ii in Figure 1b), and is zero if either monomer is uncharged (i.e., in the N state). The next term is zero if the monomer is noninteracting with a nearby charge of the opposite sign (i in Figure 1b). Both of these terms are multiplied by a factor $\Gamma_0 = \lambda_B/(2a)$ that is the strength of the Coulomb interaction between charges that are directly adjacent, where $\lambda_B = e^2/(4\pi\epsilon k_B T)$ is the Bjerrum length, e is the elementary charge, ϵ is the dielectric constant, $k_B T$ is the thermal energy, and a is the hydrated radius of the charges. The next two terms represent the interactions between a charged monomer site at i and an adsorbed charge at site $i + 1$ or vice versa, that interact with a strength $\Gamma_1 = \Gamma_0/\sqrt{2}$ that we approximate as being over a distance that is the hypotenuse of a right triangle formed by the charged species (see iii and iv in Figure 1b). The next term represents the single-bond partition functions associated with continuing to bind a run of

https://doi.org/10.1021/acs.jpcb.1c03065
J. Phys. Chem. B 2021, 125, 8965−8980

polyelectrolyte charges, with a factor of 2 for the start of the run (i.e., P′ to P) due to the choice of direction for the adsorbed chain. The final terms consist of the chemical potentials of the adsorbing polymer and salt species (given in our previous works as $\mu_{P-} = \ln B_0\phi_{P-}$ and $\mu_{S-} = \ln A_0\phi_{S-}$), as well as the reference potentials for the test polycation charge μ^0_{P+} and the uncharged monomers along the test polycation μ^0_{POH}.

Our convention is to subtract the potential in eq 2 by a reference potential $W_{ref,+} = -\sum_i 2\Gamma_1 + \mu^0_{P+}$ to yield the new expression:

$$\begin{aligned}\beta\Delta W_+(\{s_i\}) = \sum_{i=1}^{N-1} \{&-\Gamma_0[(\delta_{s_i,N} + \delta_{s_{i+1},N} - \delta_{s_i,N}\delta_{s_{i+1},N}) \\ &- (\delta_{s_{i+1},N} + \delta_{s_{i+1},0})] \\ &+ \Gamma_1[2\delta_{s_i,N} + 2\delta_{s_{i+1},N} + \delta_{s_i,0} + \delta_{s_{i+1},0} \\ &- \delta_{s_i,N}(\delta_{s_{i+1},N} + \delta_{s_{i+1},0}) - \delta_{s_{i+1},N} \\ &(\delta_{s_i,N} + \delta_{s_i,0})] - \delta_{s_i,P}\delta_{s_{i+1},P}\ln(E) \\ &- \delta_{s_i,P'}\delta_{s_{i+1},P}\ln(2E)\} \\ &- \sum_{i=0}^{N-1} \{\delta_{s_{i+1},P}\beta\mu_{P-} + \delta_{s_{i+1},S}\beta\mu_{S-} \\ &+ \delta_{s_{i+1},N}\beta(\mu^0_{POH} - \mu^0_{P+})\}\end{aligned} \tag{3}$$

It is possible to use the expression

$$\delta_{s_i,S} + \delta_{s_i,P} + \delta_{s_i,P'} + \delta_{s_i,0} + \delta_{s_i,N} = 1$$

to rewrite this energy expression as factors of either pairs of $\delta_{s_i,\sigma}\delta_{s_{i+1},\sigma'}$ that indicate that monomer i is in state σ and monomer $i+1$ is in state σ', or as factors of a single $\delta_{s_{i+1},\sigma}$ that only depends on the state of monomer $i+1$ regardless of the state of monomer i. The generalized expression is

$$\begin{aligned}\beta\Delta W_+(\{s_i\}) = &\sum_\sigma \mathcal{M}^{I}_\sigma\delta_{s_1,\sigma} \\ &+ \sum_{i=1}^{N_P-1}\left\{\sum_\sigma \mathcal{M}^{I}_\sigma\delta_{s_{i+1},\sigma} + \sum_{\sigma,\sigma'}\mathcal{M}^{II}_{\sigma,\sigma'}\delta_{s_i,\sigma}\delta_{s_{i+1},\sigma'}\right\}\end{aligned} \tag{4}$$

The first term considers the first monomer, which is otherwise left out of the bracketed sum over all N_P monomers along the chain. This more compact notation requires calculation of a number of coefficients $\mathcal{M}^{I}_\sigma$ and $\mathcal{M}^{II}_{\sigma,\sigma'}$. The first of these coefficients $\mathcal{M}^{I}_\sigma$ corresponds to the state of an individual monomer in state $\sigma = \{S, P, P', 0, N\}$, while the second of these coefficients $\mathcal{M}^{II}_{\sigma,\sigma'}$ corresponds to a sequential pair of monomers in states σ and σ'. These coefficients are determined from eq 3. We can then incorporate this into the partition function, eq 1, to yield:

$$\begin{aligned}\Xi_{int,+}(N_P) = \sum_{\{s_1\cdots s_N\}} \exp\Bigg[&-\sum_\sigma \mathcal{M}^{I}_\sigma\delta_{s_1,\sigma} \\ &- \sum_{i=1}^{N_P-1}\left\{\sum_\sigma \mathcal{M}^{I}_\sigma\delta_{s_{i+1},\sigma} + \sum_{\sigma,\sigma'}\mathcal{M}^{II}_{\sigma,\sigma'}\delta_{s_i,\sigma}\delta_{s_{i+1},\sigma'}\right\}\Bigg]\end{aligned} \tag{5}$$

We now explicitly include chain length N_P as an argument for $\Xi_{int,+}(N_P)$, and write out the summation in the exponential to explicitly include the final terms associated with monomer N_P and its interaction with $N_P - 1$:

$$\begin{aligned}\Xi_{int,+}(N_P) = \sum_{\{s_1\cdots s_N\}} \exp\Bigg[&-\sum_\sigma \mathcal{M}^{I}_\sigma\delta_{s_1,\sigma} \\ &- \sum_{i=1}^{N_P-2}\left\{\sum_\sigma \mathcal{M}^{I}_\sigma\delta_{s_{i+1},\sigma} + \sum_{\sigma,\sigma'}\mathcal{M}^{II}_{\sigma,\sigma'}\delta_{s_i,\sigma}\delta_{s_{i+1},\sigma'}\right\} \\ &- \sum_\sigma \mathcal{M}^{I}_\sigma\delta_{s_N,\sigma} - \sum_{\sigma,\sigma'}\mathcal{M}^{II}_{\sigma,\sigma'}\delta_{s_{N-1},\sigma}\delta_{s_N,\sigma'}\Bigg]\end{aligned} \tag{6}$$

We then write the portion of the partition sum that has a specified s_N:

$$\begin{aligned}\Xi_{int,+}(N_P|s_N) = \sum_{\{s_1\cdots s_{N-1}\}} \exp\Bigg[&-\sum_\sigma \mathcal{M}^{I}_\sigma\delta_{s_1,\sigma} \\ &- \sum_{i=1}^{N_P-2}\left\{\sum_\sigma \mathcal{M}^{I}_\sigma\delta_{s_{i+1},\sigma} + \sum_{\sigma,\sigma'}\mathcal{M}^{II}_{\sigma,\sigma'}\delta_{s_i,\sigma}\delta_{s_{i+1},\sigma'}\right\} \\ &- \mathcal{M}^{I}_{s_N} - \sum_\sigma \mathcal{M}^{II}_{\sigma,s_N}\delta_{s_{N-1},\sigma}\Bigg]\end{aligned} \tag{7}$$

This is related to the original partition function via the summation

$$\Xi_{int,+}(N_P) = \sum_{s_N}\Xi_{int,+}(N_P|s_N)$$

We can expand this expression to explicitly write out the $N_P - 1$ terms:

$$\begin{aligned}\Xi_{int,+}(N_P|s_N) = \sum_{\{s_1\cdots s_{N-1}\}} \exp[&-\sum_\sigma \mathcal{M}^{I}_\sigma\delta_{s_1,\sigma} \\ &- \sum_{i=1}^{N_P-3}\left\{\sum_\sigma \mathcal{M}^{I}_\sigma\delta_{s_{i+1},\sigma} + \sum_{\sigma,\sigma'}\mathcal{M}^{II}_{\sigma,\sigma'}\delta_{s_i,\sigma}\delta_{s_{i+1},\sigma'}\right\} \\ &- \sum_\sigma \mathcal{M}^{I}_\sigma\delta_{s_{N-1},\sigma} - \sum_{\sigma,\sigma'}\mathcal{M}^{II}_{\sigma,\sigma'}\delta_{s_{N-2},\sigma}\delta_{s_{N-1},\sigma'} - \mathcal{M}^{I}_{s_N} \\ &- \sum_\sigma \mathcal{M}^{II}_{\sigma,s_N}\delta_{s_{N-1},\sigma}]\end{aligned} \tag{8}$$

$$\begin{aligned}= \sum_{s_{N-1}}\Bigg\{\sum_{\{s_1\cdots s_{N-2}\}} \exp\Bigg[&-\sum_\sigma \mathcal{M}^{I}_\sigma\delta_{s_1,\sigma} \\ &- \sum_{i=1}^{N_P-3}\left(\sum_\sigma \mathcal{M}^{I}_\sigma\delta_{s_{i+1},\sigma} + \sum_{\sigma,\sigma'}\mathcal{M}^{II}_{\sigma,\sigma'}\delta_{s_i,\sigma}\delta_{s_{i+1},\sigma'}\right) \\ &- \mathcal{M}^{I}_{s_{N-1}} - \sum_\sigma \mathcal{M}^{II}_{\sigma,s_{N-1}}\delta_{s_{N-2}}\Bigg]\Bigg\}\exp\left[-\mathcal{M}^{I}_{s_N} - \mathcal{M}^{II}_{s_{N-1},s_N}\right]\end{aligned} \tag{9}$$

The term in the curly brackets is simply $\Xi_{int,+}(N-1|s_{N-1})$, and we can define a quantity

$$M_{s+1,s} = \exp[-(\mathcal{M}^{I}_{s_{i+1}} + \mathcal{M}^{II}_{s_i,s_{i+1}})]$$

to write the relationship:

$$\Xi_{int,+}(N|s_N) = \sum_{s_{N-1}} M_{s_N,s_{N-1}}\Xi_{int,+}(N-1|s_{N-1}) \tag{10}$$

https://doi.org/10.1021/acs.jpcb.1c03065
J. Phys. Chem. B 2021, 125, 8965−8980

This relationship can be recursively used, if the equivalent expression using, for example, $N-1$ and $N-2$ instead of N is used, leading to the result:

$$\Xi_{\text{int}}(N_{\text{P}}) = \sum_{s_N}\sum_{s_{N-1}}\sum_{s_{N-2}}\sum_{s_{N-3}} \cdots M_{s_N,s_{N-1}} M_{s_{N-1},s_{N-2}} M_{s_{N-2},s_{N-3}} \cdots \Xi_{int,+}(1|s_1) \tag{11}$$

This expression can be written more compactly in matrix form, using the vectors

$$\vec{\psi}_1^{\,\text{T}} = [1,1,1,1,1]$$

$$\vec{\psi}_0 = \Xi_{int,+}(1|s_1) = [A_-,\ 0,\ B_-,\ \gamma_1,\ \lambda_+\gamma_1^2]^{\text{T}}$$

and the matrix $M_{s+1,s} = \mathbf{M}$:

$$\Xi_{\text{int},+} = \vec{\psi}_0^{\,\text{T}} \mathbf{M}^{N_{\text{P}+}} \vec{\psi}_1 \tag{12}$$

Using this procedure, and starting from eqs 1 and 3, we can write this matrix as

$$M_{s_{i+1},s_i} = \begin{bmatrix} \text{SS} & \text{SP} & \text{SP}' & \text{S0} & \text{SN} \\ \text{PS} & \text{PP} & \text{PP}' & \text{P0} & \text{PN} \\ \text{P}'\text{S} & \text{P}'\text{P} & \text{P}'\text{P}' & \text{P}'0 & \text{P}'\text{N} \\ 0\text{S} & 0\text{P} & 0\text{P}' & 00 & 0\text{N} \\ \text{NS} & \text{NP} & \text{NP}' & \text{N0} & \text{NN} \end{bmatrix} = \begin{bmatrix} A_- & A_- & A_- & A_-\gamma_1 & A_-\gamma_0^{-1}\gamma_1^2 \\ 0 & E_- & 2E_- & 0 & 0 \\ B_- & B_- & B_- & B_-\gamma_1 & B_1\gamma_0^{-1}\gamma_1^2 \\ \gamma_0\gamma_1 & \gamma_0\gamma_1 & \gamma_0\gamma_1 & \gamma_0\gamma_1^2 & \gamma_1^2 \\ \lambda_+\gamma_1^2 & \lambda_+\gamma_1^2 & \lambda_+\gamma_1^2 & \lambda_+\gamma_1^2 & \lambda_+\gamma_1^2 \end{bmatrix} \tag{13}$$

The first form of the matrix indicates the pairs of states for each matrix element, with the $i+1$ state followed by the i state. Conceptually, these elements contain the Boltzmann factors for this pair of states s_{i+1} and s_i, including both the energies associated with the monomer $i+1$ as well as the energies associated with the specific pair of states on i and $i+1$. For example, the NP element $M_{N,\text{P}} = \lambda_+\gamma_1^2$ has a contribution due to the uncharged state of $s_{i+1} = \text{N}$ (the λ_+ factor) and a contribution due to the juxtaposition of the $s_i = \text{P}$ and $s_{i+1} = \text{N}$ states (the γ_1^2 factor). This latter factor accounts for the absence of the two charge−charge interactions between sites denoted by the Roman numeral arrows III and IV in Figure 1; this is a deviation from the fully charged and fully adsorbed reference state, as suggested by its definition $\gamma_1 = \exp(-\Gamma_1)$. Our notation above reflects the various exponential factors determined from eqs 3 and 9, defining $A_- = \exp(\beta\mu_{\text{S}-}) = A_0\phi_{\text{S}-}$, $B_- = \exp(\beta\mu_{\text{P}-}) = B_0\phi_{\text{P}-}$, $\gamma_0 = \exp(-\Gamma_0)$, $E_- = \langle f_{d,-}\rangle$, and $\lambda_+ = \exp[-\ln(10)(\text{p}K_{\text{a,conj}} - \text{pH})]$. The variables A_- and B_- are exponential factors related to the chemical potentials of the salt and polymer species respectively, and carry a subscript "−" to denote that the species adsorbing to a polycation test chain are negatively charged. The variable E_- was chosen as one for a fully charged adsorbing polyelectrolyte in our previous work,[148] but we instead make this equal to $\langle f_{d,-}\rangle$ to account for the possibility that the next monomer in an adsorbing weak polyelectrolyte chain may not be charged. For λ_+, we have used the dissociation reaction for the conjugate acid of the polybase:

$$\text{PH}^+ \rightleftharpoons \text{P} + \text{H}^+ \tag{14}$$

The dissociation reaction constant $K_{\text{a,conj}} = a_{\text{P}}a_{\text{H}+}/a_{\text{PH}+}$ is related to the standard state chemical potentials $\beta\mu_i^0$ of species i. Defining $\text{p}K_{\text{a,conj}} = -\log K_{\text{a,conj}}$ and $\text{pH} = -\log a_{\text{H}+}$, it is possible to obtain the above expression for $\lambda_+ = \exp[\beta(\mu_{\text{P}+}^0 - \mu_{\text{POH}}^0)]$. The corresponding value for the weak polyanion is $\lambda_- = \exp[-\ln(10)(\text{pH} - \text{p}K_a)] = \exp[\beta(\mu_{\text{A}-}^0 - \mu_{\text{AH}}^0)]$.

In the above exposition of the transfer-matrix model for interactions between a polymer and its surroundings, we considered a polycation as denoted by the subscript for $\Xi_{\text{int},+}$. However, we also note that a number of quantities (i.e., $\phi_{\text{S}-}$, $\phi_{\text{P}-}$, and $\langle f_{d,-}\rangle$) are for the opposite sign as these correspond to the species that is adsorbed to the test polymer. In a system with fixed quantities of three of the four charged species (e.g., $\phi_{\text{P}\pm}$ and $\phi_{\text{S}+}$), with the last charged species being chosen to satisfy electroneutrality, the two partition functions $\Xi_{\text{int},+}(\{\phi_i\}, \langle f_{d,-}\rangle)$ and $\Xi_{\text{int},-}(\{\phi_i\}, \langle f_{d,+}\rangle)$ are functions of the charge fraction on the oppositely charged chains and must therefore be consistent. This is because the charge fractions are themselves functions of their respective partition functions:

$$\langle f_{d,\pm}\rangle = 1 - \frac{1}{N_{\text{P}\pm}}\left(\frac{\partial \ln \Xi_{\text{int},\pm}}{\partial \ln \lambda_\pm}\right) \tag{15}$$

Here, the values of all quantities denoted with a $\pm$ can be interchanged depending on the polyelectrolyte of focus. In our calculation of these quantities, we thus iteratively solve all four equations; the two partition functions $\Xi_{\text{int},\pm}$ and the two charge fractions $\langle f_{d,\pm}\rangle$ until a consistent set of values is found.

This transfer function formalism accounts for the interaction of a test chain (in this case, both the polycation and polyanion species) in the presence of surrounding, adsorbing species of opposite charge. This can then be incorporated into the overall free energy density for a coacervate-forming solution of polyelectrolytes:

$$\begin{aligned} \frac{\mathcal{F}}{Vk_{\text{B}}T} = {} & \frac{\phi_{\text{P}+}}{N_{\text{P}+}}\ln\phi_{\text{P}+} + \frac{\phi_{\text{P}-}}{N_{\text{P}-}}\ln\phi_{\text{P}-} + \sum_{\alpha=W,+,-}\phi_\alpha \ln\phi_\alpha \\ & - \frac{\phi_{\text{P}+}}{2N_{\text{P}+}}\ln\Xi_{\text{int,P}+} - \frac{\phi_{\text{P}-}}{2N_{\text{P}-}}\ln\Xi_{\text{int,P}-} \\ & + \zeta\left[\Lambda(\phi_{\text{P}+} + \phi_{\text{P}-}) + \sum\nolimits_{\alpha=+,-}\phi_\alpha\right]^3 + \zeta_{es} \\ & [\langle f_{d,\text{P}+}\rangle\phi_{\text{P}+} + \phi_{\text{S}+} + \phi_{\text{H}+} - \langle f_{d,\text{P}-}\rangle\phi_{\text{P}-} - \phi_{\text{S}-} - \phi_{\text{OH}-}]^2 \end{aligned} \tag{16}$$

This free energy includes the configurational entropy of mixing in the first three terms (for all polyelectrolyte, salt, and water species), the interaction free energies as determined by the transfer matrix theory in terms four and five, and then two final terms reflecting excluded volume and an electroeutrality constraint, respectively. We do note that the free energy of interaction

$$\mathcal{W}_{\text{int},\pm} = -k_{\text{B}}T\ln\Xi_{\text{int},\pm}$$

that comes from the transfer matrix theory is a grand potential, as the test chain system boundary is open to the adsorption of external salt species and pH effects; however, this can be incorporated directly into the overall Helmholtz free energy $\mathcal{F}$. An equivalent interpretation of this test chain subsystem is that the adsorption processes for monomer states S and P′ are simply alternative states with an effective energy $\epsilon_{\text{eff}} = \epsilon - \mu$ such that there is a corresponding canonical partition function leading to a Helmholtz free energy of interaction. We also mention that it is this term that includes the electrostatic interactions, with a

https://doi.org/10.1021/acs.jpcb.1c03065
J. Phys. Chem. B 2021, 125, 8965−8980

strength determined by the dimensionless Bjerrum lengths Γ_0 and Γ_1 in eq 3. The excluded volume term is a phenomenological cubic term that accounts for the packing free energy at high volume fractions, which is significant for coacervates where the volume of nonwater species can be as high as 10−30%.[90] We distinguish this term from pairwise interactions and pairwise excluded volume, in that it represents higher-order repulsions between charged species; two-body interactions would instead be included either in the transfer matrix calculation as a pairwise energy between adsorbing species or as an added χ contribution to the free energy.[154] The final term in eq 16 is needed to ensure electroneutrality, since our MC numerical scheme does not strictly maintain this constraint. We instead use this quadratic term to energetically penalize a net positive or negative charge in each phase, relying on the overall minimization of the free energy to obtain an electroneutral state. We thus use a large constant $\zeta_{es} = 50.0$ to strongly favor states where the positive and negative species are equivalent.

We note that, in this free energy expression, we assume that the local concentration of H+ and OH− species is the same as that in the reservoir and thus do not explicitly include (for example) the corresponding translational entropy terms. Here, ϕ_{H+} and ϕ_{OH-} are simply the concentrations expected at a given pH. This may not be the case, as has been demonstrated in prior work by Szleifer et al., where the local concentration of H+ and OH− is affected by the local electrostatic potential.[143,145] We could modify our formalism to account for the equilibrium between the reservoir and the system, but in our case we neglect this effect by virtue of the highly screened electrostatic interactions.[145] To justify this approximation, we note first that the volume fraction of H+ and OH− charges is much smaller than the other charged species; using a typical species volume ($\nu_{H+} = 0.03$ nm)[145] we can calculate that $\phi_{H+} = 1.8 \times 10^{-4}$ even at a low pH = 2. This is almost three orders of magnitude lower than the typical concentrations $\phi_{P\pm} + \phi_{S\pm} \sim 0.1$ observed in the coacervate phase. Furthermore, the screening length for a typical concentration of charged species in the coacervate phase (∼1.5M),[90] is unphysically low ($\kappa^{-1} \approx 0.3$ nm); this is indicative of the failure of Debye-Hückel at these concentrations, where charge interactions are highly localized.[107]

We calculate phase boundaries in this model using a numerical procedure designed to determine coexisting states. This is not trivial, as the charge state of the polymers and thus the balance of ions needed to maintain electroneutrality can change drastically upon phase separation. In addition, these components must conserve mass from a physically realizable initial state. To simply meet this criteria, we choose the density of three out of four of the charged species (ϕ_{P+}, ϕ_{P-}, and either ϕ_{S+} or ϕ_{S-}), and set the density of the other salt species to be electroneutral. We then solve for the partition functions $\Xi_{int,+}$ and $\Xi_{int,-}$, which may affect the $\langle f_{d,+}\rangle$ or $\langle f_{d,-}\rangle$ respectively. This will then alter the electroneutrality condition for calculating the variable salt species. This procedure is performed iteratively, until the system is electroneutral and is internally consistent with respect to the polymer charge fractions, and we obtain a homogeneous state that serves as a starting point for phase separation. We subsequently consider two "systems" at this homogeneous starting state and perturbatively moving random amounts of each species between the systems via Monte Carlo updates, until a minimum free energy for both systems combined is attained. While this approach has the advantage of determining phase coexistence in this many-component system while maintaining electroneutrality and acid−base equilibria, we note that the stochastic nature of this calculation can lead to small variations in the location of phase boundaries. We use parameters that have been demonstrated to work well in previous versions of the transfer matrix theory: $A_0 = 41.0$, $B_0 = 24.4$, $\zeta = 19.0$, and $\Lambda = 0.6875$. We will vary Γ_0, but will choose to run most calculations with $\Gamma_0 = 1.75$. Finally, to consider the common polypeptides poly(aspartate) and poly(lysine), we will use pK_a (or $pK_{a,conj}$) values of 3.9 and 10.5, respectively, emphasizing that these are the monomer pK_a values, and not the effective pK_a values that we will eventually obtain from our polymer model.

RESULTS AND DISCUSSION

The transfer matrix approach articulated in the methods section is intended to model pH-dependent complex coacervation; however, the success of this formalism hinges upon its ability to more generally capture phenomenology associated with weak polyelectrolytes. We will first show that this model captures a variety of important effects known to affect weak polyelectrolyte systems, and these concepts will subsequently inform our predictions for pH-effects in coacervation. Specifically, we will systematically increase the complexity in our transfer matrix model, and quantify the fraction of dissociated (i.e., charged) monomers as a function of pH. We will start from an "ideal" polyelectrolyte without interactions between charged monomers and their neighbors or oppositely charged species (Figure 2a). Subsequently, we will add in neighboring monomer interactions (Figure 2b), salt species (Figure 2c), and finally oppositely charged polyelectrolytes (to obtain systems such as the one shown schematically in Figure 1a).

Fraction of Dissociated Charges versus pH. The transfer matrix formalism is capable of calculating the fraction of charged monomers $\langle f_{d,\pm}\rangle$ on both the polycations and polyanions, via the expression given in eq 15.

We first calculate $\langle f_{d-}\rangle$ and $\langle f_{d+}\rangle$ for dilute, weak electrolytes, where the charges are noninteracting and only participate in the acid−base equilibrium. Here, we can take the limit that $\Gamma_0 \to 0$ ($\gamma_0 = 1$), $\Gamma_1 \to 0$ ($\gamma_1 = 1$), $A_\pm \to 0$, and $B_\pm \to 0$. We use the $\pm$ in the subscript to indicate the quantities for either polycation and polyanion species. In this case, the states S, P, and P′ are not possible, so we end up with the simplified matrix:

$$M_{s_{i+1},s_i} = \begin{bmatrix} 00 & 0N \\ N0 & NN \end{bmatrix} = \begin{bmatrix} 1 & 1 \\ \lambda_\pm & \lambda_\pm \end{bmatrix} \tag{17}$$

Here, the eigenvalue of this transfer matrix simplifies to the trivial result $\xi_\pm = 1 + \lambda_\pm$, such that $\Xi_\pm = (1 + \lambda_\pm)^{N_\pm}$. From this, it is straightforward to evaluate the charge dissociated, which for a polycation would be

$$\langle f_{d,-}\rangle = \frac{1}{1 + \lambda_-} = \frac{1}{1 + [H+]/K_a} \tag{18}$$

This is the classical Henderson-Hasselbalch result, which emerges from this formalism in the appropriate limit of a dilute electrolyte. We plot this curve for both the positively and negatively charged electrolytes in Figure 3, indicating that pH = pK_a for the polyanion corresponds to the point at which $\langle f_{d-}\rangle = 0.5$, and that pH = $pK_{a,conj}$ for the polycation corresponds to the point at which $\langle f_{d+}\rangle = 0.5$. This reflects the acid−base equilibrium in an "ideal", dilute electrolyte situation, and we include the Henderson-Hasselbalch result in all plots in Figure 4

https://doi.org/10.1021/acs.jpcb.1c03065
J. Phys. Chem. B 2021, 125, 8965−8980

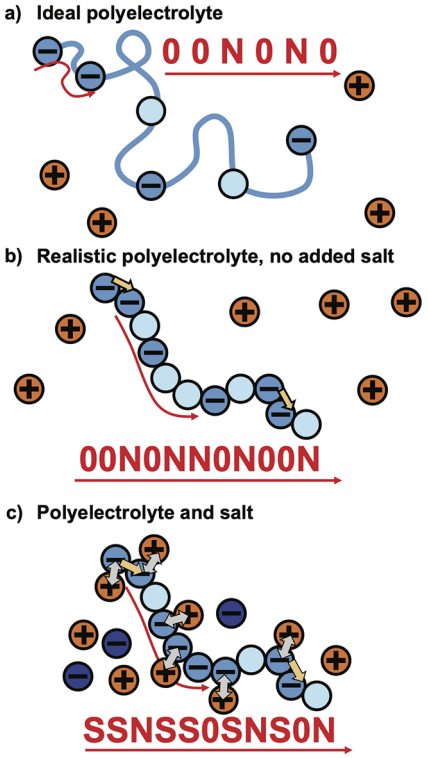

Figure 2. We can systematically vary the role of specific interactions in our transfer matrix model. In panel a, we consider an "ideal" polyelectrolyte, where the monomers are sufficiently far apart that there is negligible energetic penalty for adjacent charged monomers, and the salt is sufficiently dilute that the "S" state is unobserved. Charge fraction $\langle f_{d,-}\rangle$ in this case follows the Henderson-Hasselbalch prediction. In panel b, adjacent charged monomers have an energetic penalty (tan arrows), suppressing the charging of these polyelectrolytes to higher pH values (for polyanions) or lower pH values (for polycations). In this case, we still consider negligible salt, which is finally included in panel c. This has the effect of promoting polyelectrolyte charging, due to favorable interactions (blue arrows) with oppositely charged salt ions.

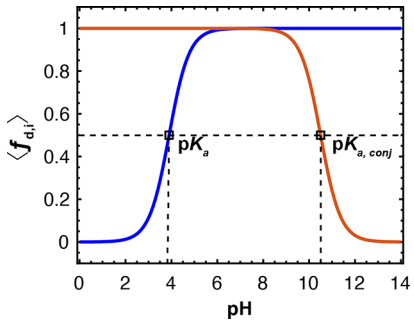

Figure 3. Ideal Henderson-Hasselbalch result for the polyelectrolytes i considered in this paper, plotting the fraction dissociated $\langle f_{d,i}\rangle$ versus the solution pH. The polyanion species (blue) represents poly(lysine) with a $pK_a = 3.9$, which corresponds to the monomer at $\langle f_{d,-}\rangle = 0.5$ at a pH = 3.9. The polycation species (orange) represents poly(aspartate) with a $pK_{a,conj} = 10.5$. Because these species are symmetric, we will focus on the low-pH region and effects related to the weakly charged polyanion.

(black curves) for comparison with nonideal results. Figure 3 also demonstrates the symmetry between the polyanion and polycation; we will focus on the low-pH region and effects related to the weakly charged polyanion in the subsequent discussion, though the same physical concepts are also expected to apply to the weakly charged polycation.

This result can be incrementally modified by including the along-the-chain repulsion between charged monomers, by increasing the value of $\Gamma_0 > 0$ so that $\gamma_0 \leq 1$. We still consider dilute polyelectrolytes such that oppositely charged salt and polymeric species are at negligible concentrations, so we retain the simplified matrix for the previous case with only slight modification:

$$M_{s_{i+1},s_i} = \begin{bmatrix} 00 & 0N \\ N0 & NN \end{bmatrix} = \begin{bmatrix} \gamma_0 & 1 \\ \lambda & \lambda \end{bmatrix} \tag{19}$$

Here, we end up with a largest eigenvalue

$$\xi_\pm = [\lambda_\pm + \gamma_0 + \sqrt{(\lambda_\pm + \gamma_0)^2 - 4\lambda_\pm(\gamma_0 - 1)}\,]/2$$

leading to an analytical expression for the dissociation as a function of pH:

$$\langle f_{d,-}\rangle = 1 - \frac{\lambda}{\xi_-}\left[\frac{\xi_- - \gamma_0 + 1}{\sqrt{(\lambda_- + \gamma_0)^2 - 4\lambda_-(\gamma_0 - 1)}}\right] \tag{20}$$

Here, we write the expression for a polyanion, but could simply switch the subscript signs to write this for a polycation. We plot $\langle f_{d,-}\rangle$ versus pH in Figure 4a, demonstrating how a polyelectrolyte undergoes a charging transition as $\Gamma_0 = -\ln \gamma_0$ is increased from $\Gamma_0 = 0$ to 1.75, along with the ideal Henderson-Hasselbalch result (black curve). Γ_0 increases the repulsion between adjacent charges along the chain backbone, which penalizes the fully charged state and decreases the pH at which the polymer chain charges. This penalty is more significant at higher charging, leading to a broadening of the dissociation transition when compared to Henderson−Hasselbalch consistent with simulation results by Rathee et al.[88]

This trend toward the suppression of polyanion charging can be mitigated—and even reversed—upon introduction of salt into the system. For this single-polyelectrolyte system, we still neglect the presence of other, oppositely charged chains (i.e., no P or P′ states), and end up with a 3 × 3 matrix:

$$M_{s_{i+1},s_i} = \begin{bmatrix} SS & S0 & SN \\ 0S & 00 & 0N \\ NS & N0 & NN \end{bmatrix} = \begin{bmatrix} A_- & A_-\gamma_1 & A_-\gamma_0^{-1}\gamma_1^2 \\ \gamma_0\gamma_1 & \gamma_0\gamma_1^2 & \gamma_1^2 \\ \lambda\gamma_1^2 & \lambda\gamma_1^2 & \lambda\gamma_1^2 \end{bmatrix} \tag{21}$$

We choose to evaluate the corresponding partition function and prediction for the dissociation fraction numerically, and plot the result in Figure 4b. A small increase in salt concentration $\phi_{S-} \leq 2 \times 10^{-3}$ (or roughly 20 mM assuming a hydrated ion radius of 0.35 nm) promotes the charging of the polycation, counteracting the degree to which charging is prevented by the along-the-chain like-charge repulsion. Further increase in salt concentration above this point *promotes* charging in our model, due to the additional favorable interaction between the charged monomer and the localized counterions on neighboring monomers. This leads to a significant shift to low $pK_{a,eff}$ values at high, coacervate-relevant salt concentrations.

This charging effect can be exacerbated by the presence of nearby polyelectrolyte chains, for which we must use the full transfer matrix in eq 13. We plot in Figure 4 panels c and d the dissociation fraction on the polyanion for a number of polycation concentrations ϕ_{P+}, assuming a constant salt ϕ_{S-} =

https://doi.org/10.1021/acs.jpcb.1c03065
J. Phys. Chem. B 2021, 125, 8965−8980

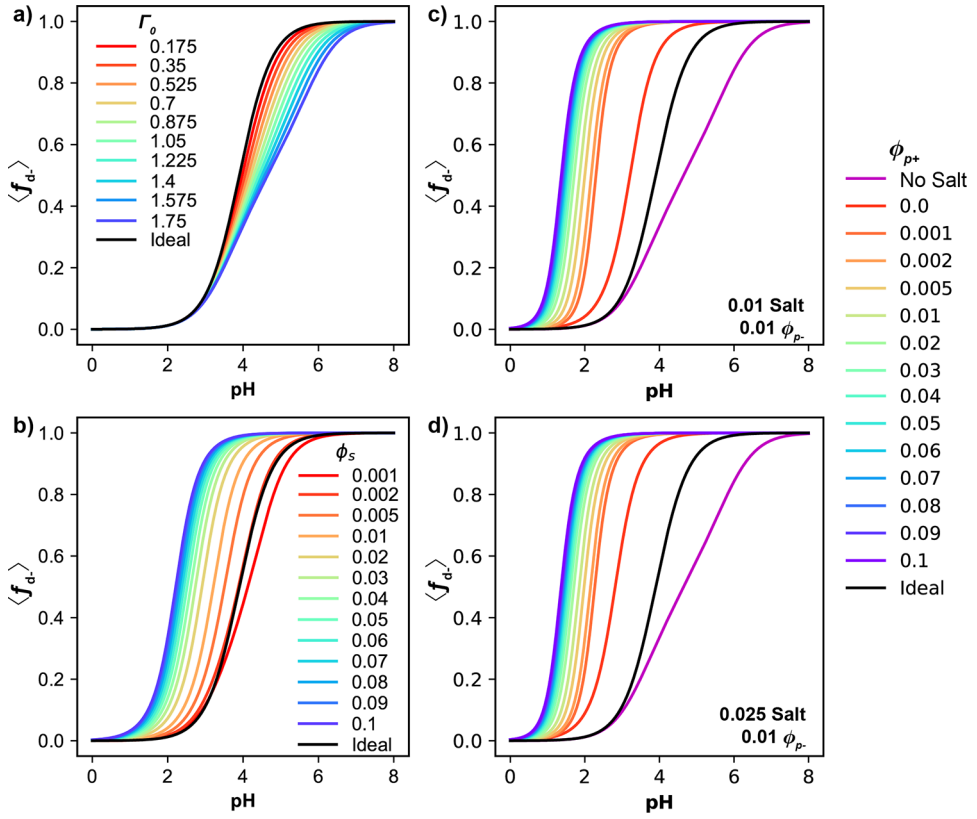

Figure 4. Plots showing the fraction of dissociated monomers on the polyanion $\langle f_{d-} \rangle$ as a function of pH. (a) Starting from the Henderson–Hasselbalch limit (black), we increase the energy penalty of adjacent charges along the same chain Γ_0. This suppresses charging of the polyanion to higher pH values. (b) At $\Gamma_0 = 1.75$, the salt concentration ϕ_{S+} is increased, ultimately facilitating the charging of the polyelectrolyte chains due to the favorable interactions between charged polyanion monomers and adjacent cations. Panels c and d consider the increase of polyelectrolyte concentration at $\phi_S = 0.01$ and $\phi_S = 0.025$, respectively. Magenta curves represent the salt $\phi_S \to 0$ limit for comparison. The cooperative effect of connected polycation charges facilitates significant charging of the polyanion even at low concentrations.

0.01 and $\phi_{S-} = 0.025$. We note here that the concentration of polyanion ϕ_{P-} does not significantly affect these results, because the polycation is fully charged at this point regardless of the charged-state of the polyanion. Here we fix a constant $\phi_{P-} = 0.01$.

The polyanion, essentially regardless of a *finite* polycation concentration, exhibits a significant shift of its $pK_{a,eff}$ to lower values. This is indicative of the cooperative effect of bound polyanion/polycation pairs, for which the presence of a bound pair of monomers facilitates the binding of the adjacent monomers. This is similar to behavior described by Salehi and Larson,[141] and consistent with observations by a number of experimental groups that significant charging can be induced in weak polyelectrolytes by oppositely charged polyelectrolytes.[153,155] Consistent with those prior observations, strongly favorable interactions arise due to the correlated charges between complexing monomers, which shift $pK_{a,eff}$ to lower values and exhibit a sharp transition to a fully charged state. At low ϕ_{P+}, this effect can be significantly affected by the salt concentration ϕ_S as seen in the differences between Figure 4 panels c and d, though at high ϕ_{P+} these two figures become essentially indistinguishable as polymers govern the charging $\langle f_{d-} \rangle$ of the polyanion.

Weak Coacervate Phase Behavior. The charge state of polyelectrolytes in our model emerges from the transfer matrix formalism, which is a key component of our coacervate model and contributes to the system free energy (eq 16). We can use this free energy to plot phase diagrams that demarcate the region of two-phase coexistence between coacervate and supernatant phases. Standard coacervation phase diagrams are typically shown on a salt concentration, ϕ_S, versus polymer concentration, ϕ_P, plot, with the assumption that charged species are symmetric such that $\phi_{S+} = \phi_{S-} = \phi_S/2$ and $\phi_{P+} = \phi_{P-} = \phi_P/2$. We plot essentially the same phase diagram in Figure 5, which at pH = 7 is fully charged for both polyelectrolytes. This constraint simplifies this system by decreasing the number of effective components to three (rather than the actual number of components, five). This approximation is reasonable for simulation or theoretical models, and has been useful in the context of experimental systems; while a few polyelectrolyte pairs have been synthesized to minimize chemical difference,[156,157] it remains an active area of research to determine how chemical differences between the polyanion/polycation can affect phase behavior.[154] Nevertheless, significant progress has been made while neglecting these differences in most coacervate models.

Weak polyelectrolytes cannot utilize this convenient assumption of symmetry, because both polymers may have very different responses to the pH of the solution. There are five regimes relevant to weak polyelectrolyte behavior; in the mid-pH range, both polyelectrolytes are fully charged. At the extreme high and low pH values, one of the polyelectrolytes is charged while the other is uncharged (for example, the polyanion at low pH). There are two transition regimes in which one of the polyelectrolytes is only partially charged. In all but the fully charged regime, the differences in charge between the

https://doi.org/10.1021/acs.jpcb.1c03065
J. Phys. Chem. B 2021, 125, 8965−8980

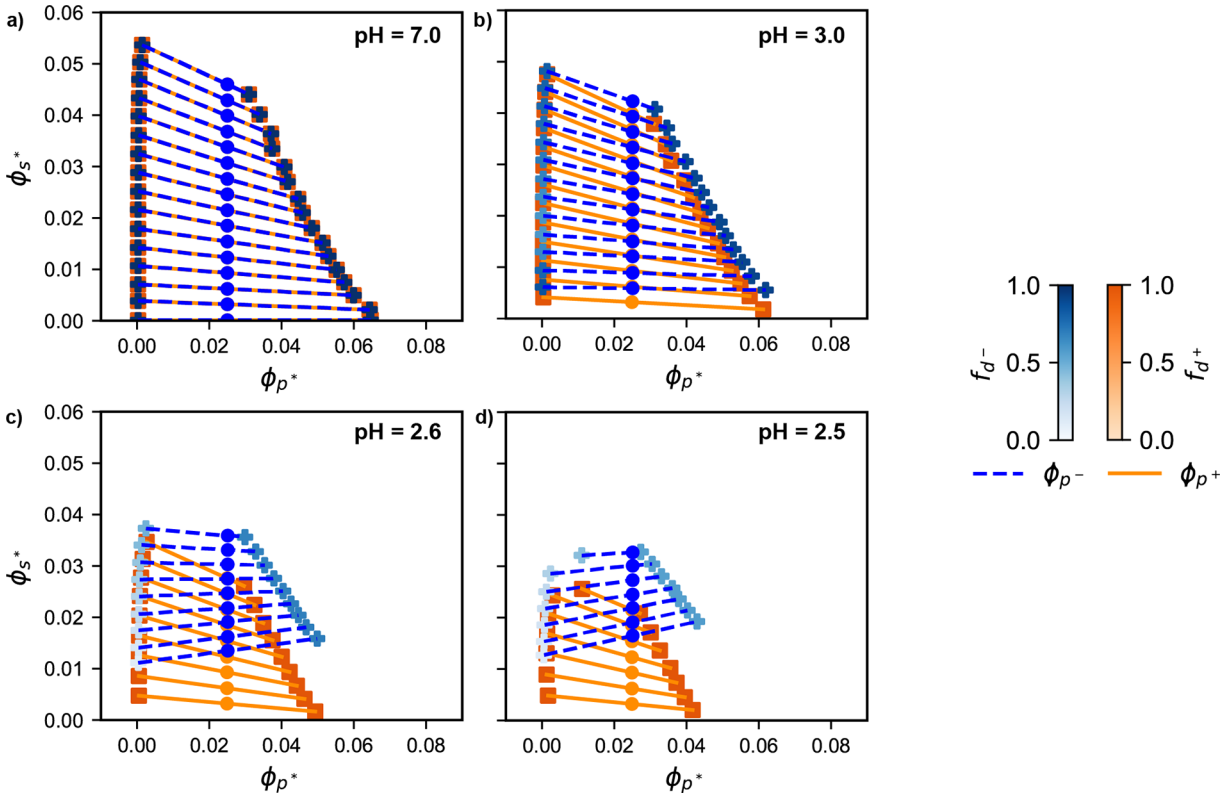

Figure 5. Phase diagrams of coacervation on the ϕ_{S*} versus ϕ_{P*} plane. Blue crosses, tie-lines correspond to negatively charged species (ϕ_{S-}, ϕ_{P-}) and the orange squares, tie-lines correspond to positively charged species (ϕ_{S+}, ϕ_{P+}). Blue and orange circular points denote the starting concentration of their respective salt, polymer species, with the polymers chosen to be at equal (i.e., stoichiometric) starting concentrations. (a) At pH = 7.0, both polymeric species are fully charged, making this identical to the typical phase diagram of a strong polyelectrolyte coacervate. All of the pH < 7.0 phase diagrams ((b) pH = 3.0, (c) pH = 2.6, and (d) pH = 2.5) exhibit deviations in charge fraction, which is reflected by the shading of the points. As pH lowers, the polyanion becomes less charged in the coacervate, and essentially uncharged in the supernatant; this reflects both the change in pH as well as the increase in $pK_{a,eff}$ when the oppositely charged species are at low concentration. The location of the binodal points is increasingly different between the two species, with small molecule anions recruited to the coacervate phase to account for the lower polyanion charge fraction.

polyelectrolytes breaks the symmetry between the two chains, necessitating changes in the phase diagram to account for all five species.

In this paper, we plot the phase behavior of weak polyelectrolytes with a pair of simultaneous diagrams that correspond to the positively and negatively charged species, respectively, allowing us to represent all five species concentrations on a single graph. This is shown for a number of values of pH in Figure 5a−d, which plot the volume fractions of salt ϕ_{S*} versus polymer ϕ_{P*} for both the positive (* = +, blue points and solid tie lines) and negative (* = −, orange points and dashed tie lines) species. This allows us to read the concentration of the four charged species directly off of the graph, while also being limited to the standard symmetric phase diagram when both species are charged (Figure 5a, pH = 7). We additionally change the shading of the points reflecting the coexisting points to show the fraction of monomers dissociated. We also denote with circular points the starting concentrations of each polyelectrolyte species used in our numerical scheme for determining binodal points, taken at $\phi_{P+} = \phi_{P-} = 0.025$. This is the concentration condition at which we first ensure that electroneutrality is maintained by adding either excess anions or cations while we equilibrate the fraction of dissociated monomers, before allowing the polymer and salt components to undergo phase separation while maintaining species conservation.

We see that, at pH = 7 (Figure 5a), we obtain the phase diagram predicted for symmetric, strongly charged polyelectrolytes, which has been demonstrated in a large number of previous works.[127] Key features include symmetry between the polycation/polyanion and cation/anion species in the location of the coexisting concentrations, which behave essentially identically. The negative slope of the tie lines emerges due to the preference of salt to partition into the supernatant phase (i.e., the left branch of the binodal curve), with these points being at a higher salt concentration than the points along the coacervate branch of the binodal. This behavior has previously been attributed to a combination of excluded volume and electrostatic interactions.[100,101,126,129,148,158]

Phase diagrams begin to deviate from the strongly charged limit upon approaching the $pK_{a,eff}$ of one of the species, in this case approaching low pH values well below the pK_a of the polyanion monomer (pK_a = 3.9). As demonstrated in the previous section, the $pK_{a,eff}$ is significantly lower due to the cooperative charging of oppositely charged polyelectrolytes, so the deviations only become apparent at pH ≈ 3.0, plotted in Figure 5b. Subsequent decreases in pH (Figure 5c,d) increasingly deviate in a number of ways; first, the supernatant at low salt concentrations exhibits a marked decrease in the fractional charge dissociation $\langle f_{d,-} \rangle$. This occurs due to the dearth of oppositely charged polycations, which would otherwise cooperatively promote polyanion charging due to charge correlations. This is effectively the case of a single dilute polyelectrolyte, where charging is suppressed by the charge repulsion between adjacent monomers. The dilute-phase

https://doi.org/10.1021/acs.jpcb.1c03065
J. Phys. Chem. B 2021, 125, 8965−8980

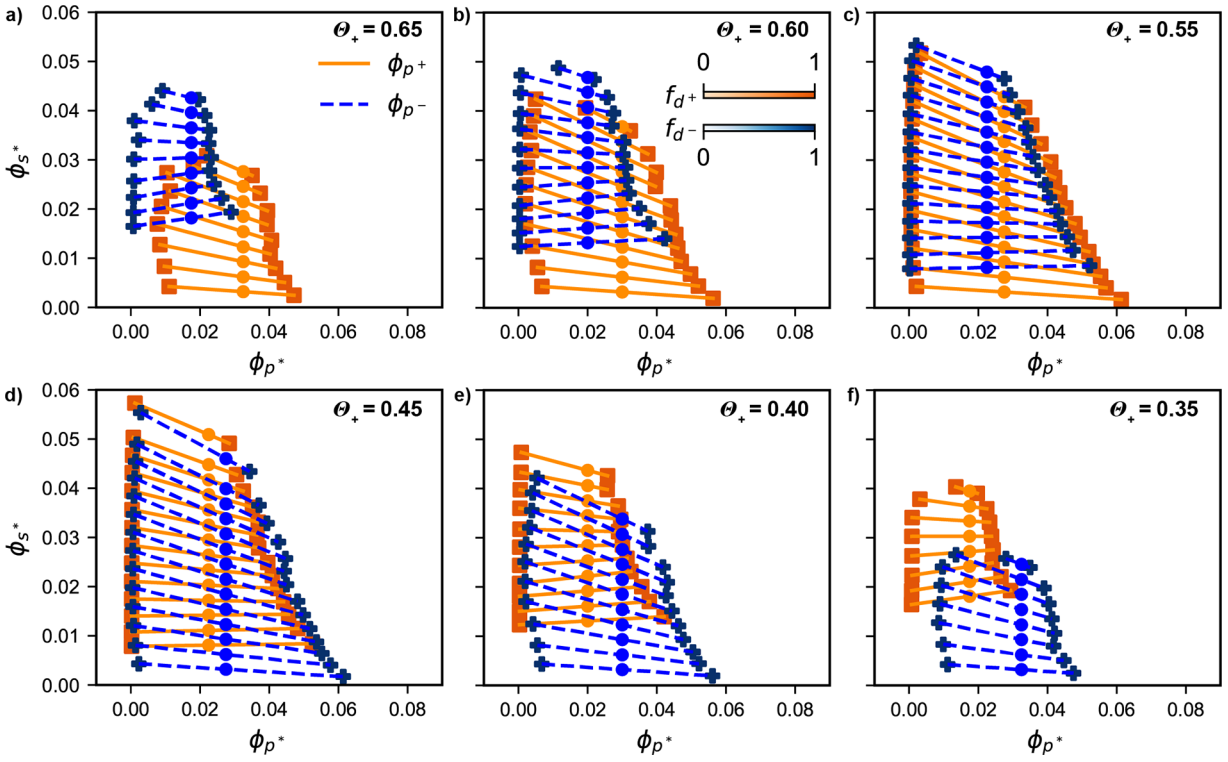

Figure 6. Phase diagrams of coacervation on the ϕ_{S*} versus ϕ_{P*} plane, for pH = 7.0 and off-stoichiometric starting mixtures of polyelectrolytes. Blue points, tie-lines correspond to negatively charged species (ϕ_{S-}, ϕ_{P-}) and the orange points, tie-lines correspond to positively charged species (ϕ_{S+}, ϕ_{P+}). Blue and orange circular points denote the starting concentration of the salt and polymer species of the respective charges. Θ_+ corresponds to the mole fraction of polycation species in the initial solution, before phase separation. (a) $\Theta_+ = 0.65$, (b) $\Theta_+ = 0.60$, (c) $\Theta_+ = 0.55$, (d) $\Theta_+ = 0.45$, (e) $\Theta_+ = 0.40$, and (f) $\Theta_+ = 0.35$. We note that the largest two-phase region occurs close to stoichiometric matching of the two species, $\Theta_+ = 0.5$, which is shown in Figure 5a. Vertical shifting of one of the species is indicative of the excess small-molecule ions needed to maintain electroneutrality for $\Theta_+ \neq 0.5$, and we note that the phase diagrams are antisymmetric around that same point due to both polyelectrolytes being essentially fully charged at pH = 7.

polyanion becomes increasingly charged as the salt increases, as a high concentration of salt will promote charging via polyanion−cation attractions. This trend toward decreasing polyanion charge is also evident in the coacervate phase, though to a lesser degree, as pH is decreased to 2.6 and 2.5.

The coacervate phase exhibits a split between the polyanion/anion and polycation/cation points, with the partially charged polyanions being at similar concentrations as the polycations ($\phi_{P+} \approx \phi_{P-}$), but with the coacervate phase having a higher anion than cation concentration ($\phi_{S-} > \phi_{S+}$). This is required for electroneutrality, as less of the polyanion is charged so it cannot neutralize the fully charged polycation at near-equivalent concentrations. There is a significant decrease in the charge fraction $\langle f_{d,-} \rangle$ of the polyanion as pH is lowered, increasing the amount of excess anion that is incorporated into the coacervate phase. This is concomitant with (1) a decrease in the extent of the two-phase region, with the coacervate exhibiting a lower polymer density as it expands due to the translational entropy of the excess anions, and (2) a depletion of the anion species in the supernatant. This latter effect narrows the extent to which $\phi_{S-} > \phi_{S+}$ in the supernatant in comparison with the coacervate.

Off-Stoichiometry Weak Coacervate Phase Diagrams. In the previous section, we considered coacervate-forming solutions consisting *initially* of equal concentrations of polycation and polyanion ($\phi_{P+} = \phi_{P-}$). However, this is merely a way to limit the set of physical parameters that we are considering, simplifying the graphical representation. This has the added benefit of simplifying to the standard symmetric case for pH values (e.g., pH = 7) where both polyelectrolytes are fully charged. We can relax this constraint, however, and explore different mole fractions $\Theta_+ = \phi_{P+}/(\phi_{P+} + \phi_{P-})$ of polycation within the total polyelectrolyte concentration. This will affect the balance of polyelectrolytes and counterions, as they partition into the two phases.

We first consider the fully charged case (pH = 7.0), for a range of values Θ_+ that deviate from the $\Theta_+ = 0.5$ case in Figure 5a, in Figure 6. We note that even small deviations, $\Theta_+ = 0.45$ and 0.55, already show significant differences from the stoichiometric cases. The species in excess remains in roughly the same place, while the other species shifts upward. This is because the species that has a lower overall volume fraction makes up for this by including more counterions in the original solution, placing points higher up along the *y*-axis. This trend continues as the value of Θ_+ moves away from 0.5, and in our model there is appropriately antisymmetry between the two species depending on the direction Θ_+ changes from the stoichiometric case. In all cases, the vertical shift between the polyelectrolyte species is attributed to the large amount of salt needed to render the overall system (i.e., both phases together) electroneutral when there is a deficiency of one of the species.

We next consider a case closer to $pK_{a,eff}$ (pH = 2.6, Figure 7), but now in a shifted range of values of $\Theta_+ = 0.15$−0.55. The shifted range accounts for the decrease in fractional charge of the polyanion, $\langle f_{d,-} \rangle < 1$, meaning that electroneutrality in the coacervate phase can in part occur by either having more polyanions than polycations ($\phi_{P-} > \phi_{P+}$) or having an excess of salt anions. At values of $\Theta_+ < 0.5$, the former condition is realized, leading to smaller vertical shifts due to excess salt

https://doi.org/10.1021/acs.jpcb.1c03065
J. Phys. Chem. B 2021, 125, 8965−8980

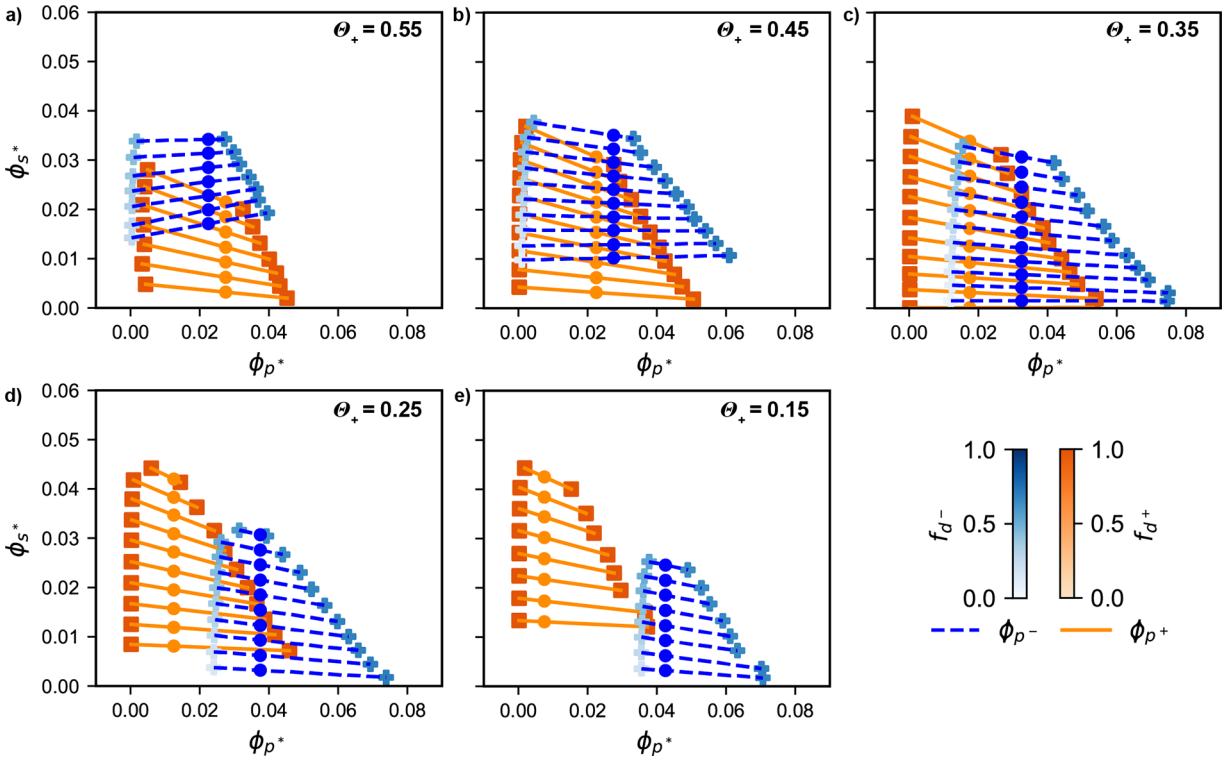

Figure 7. Phase diagrams of coacervation on the ϕ_{S*} versus ϕ_{P*} plane, for pH = 2.6 and off-stoichiometric starting mixtures of polyelectrolytes. Blue points, tie-lines correspond to negatively charged species (ϕ_{S-}, ϕ_{P-}) and the orange points, tie-lines correspond to positively charged species (ϕ_{S+}, ϕ_{P+}). Blue and orange circular points denote the starting concentration of the salt and polymer species of the respective charges. We consider a different range of Θ_+ values compared to Figure 6: (a) $\Theta_+ = 0.55$, (b) $\Theta_+ = 0.45$, (c) $\Theta_+ = 0.35$, (d) $\Theta_+ = 0.25$, and (e) $\Theta_+ = 0.15$. We note that the largest two-phase region occurs away from a stoichiometric balance of the two species, at $\Theta_+ = 0.35$. We attribute this to the partially charged polycation, indicated by the lighter shade of blue at all values of Θ_+ that means that $\langle f_{d-} \rangle < 1$; more polyanion is needed for the polyelectrolyte species themselves to be electroneutral. Vertical shifting of one of the species occurs as Θ_+ deviates from 0.35, requiring more of one of the small molecule ions to maintain electroneutrality.

between the positive/negative species at an off-stoichiometric value of $\Theta_+ = 0.35$ (Figure 7c). Here there are more polyanionic than polycationic species, so charge stoichiometry is achieved between the fully charged polycation with the (approximately) half-charged polyanion. This leads to a shift in the phase diagrams for the positive versus negative species in the *x*-direction, but there is a negligible shift in the *y*-direction because salt is not needed to make up the difference in charge between the two systems.

As the value of Θ_+ deviates from $\Theta_+ = 0.35$, the characteristics of moving to nonstoichiometric values for pH = 7.0 are also observed in this case. The positive or negatively charged polyelectrolyte in excess extends to low concentrations of its corresponding salt ion (for both the coacervate and supernatant phases), but the other species is (like in the pH = 7.0 case) in smaller quantities and needs to recruit small-molecule species to become electroneutral. This causes the phase boundaries for these species to be shifted in the *y* direction, due to the relative abundance of salt.

A major difference here is that the value of $\Theta_+ = 0.35$ at which there is charge stoichiometry in the coacervate phase exhibits a horizontal shift between the positive and negative species. This is a straightforward result of the excess of polyanion needed for electroneutrality due to its being half-charged. However, while the pH = 7.0 case led to either an antisymmetric increase in either the polycation or polyanion as Θ_+ deviated from the optimal $\Theta_+ = 0.5$ value, in this pH = 2.6 case the deviation from the optimal $\Theta_+ = 0.35$ value only changes the excess amount of polyanion except for the case where $\Theta_+ > 0.5$ (in Figure 7a).

Optimizing Polyelectrolyte Stoichiometry in Weak Coacervates. Coacervates formed from weak polyelectrolytes in experiment can determine the presence of coacervate formation via measurements of turbidity or via microscopy to determine the presence of coacervate droplets;[1,6,134] these are indirect and related measurements that rely on light scattering of coacervate droplets, are rapid to perform and largely consistent with alternative methods for determining phase coexistence.[2,10,100,101,134] In part due to the ease of probing coacervate with turbidity specifically, it is used to determine the optimal ratios of polymers for coacervation.[1,159] This is important in asymmetric systems, where the assumption that equivalent moles of each species is optimal for undergoing coacervation breaks down.

We observed this type of asymmetry in the previous section, with phase diagrams at pH = 2.6 exhibiting characteristics of equal charge stoichiometry when $\Theta_+ \neq 0.5$. This has been observed experimentally; Perry et al. demonstrated this effect for polyelectrolytes near their pK_a,[1] showing that an excess of the half-charged polyelectrolyte is needed to form a coacervate with a fully charged polyelectrolyte. They performed a series of turbidity measurements under a variety of polymer concentration ratios, at a number of different salt concentrations.

We performed the analogous calculation with our model, plotting in Figure 8a the difference in water concentration between the supernatant and coacervate, $\Delta\phi_W$, as a function of

https://doi.org/10.1021/acs.jpcb.1c03065
J. Phys. Chem. B 2021, 125, 8965−8980

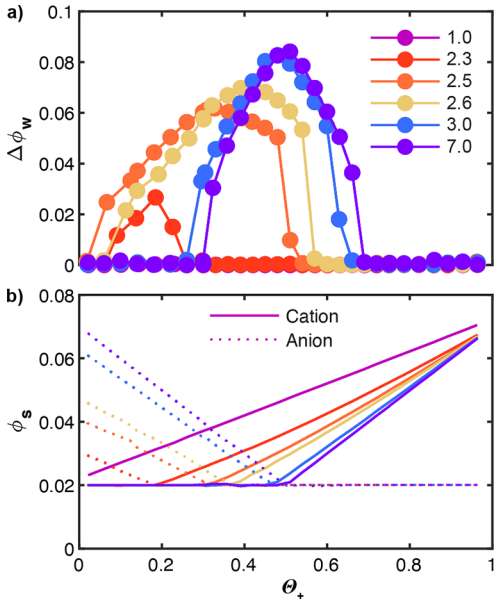

Figure 8. (a) Plot of $\Delta\phi_W$ versus Θ_+ for a number of pH values. A proxy for the presence of coacervation, analogous to conventional turbidity experiments, a shift in the optimal Θ_+ moves toward systems with more polyanion as the charge on the polyanion $\langle f_{d,-}\rangle$ decreases. The overall system is kept at a constant polymer concentration of $\phi_{P+} + \phi_{P-} = 0.05$, and the salt concentrations are plotted in panel b for both the cation and anion species. The minority salt ion is kept at $\phi_{S*} = 0.02$, while the excess of the other salt ion is chosen to keep the system electroneutral.

the mole fraction of polycation Θ_+ for a range of pH values. Our protocol is similar to what is done in experiments, in which a series of mole fractions are chosen and mixed with a predetermined amount of salt.[86,96,97] While turbidity is related to a number of physical characteristics such as droplet size, refractive index contrast, and phase separation kinetics, we consider $\Delta\phi_W$ to be a useful proxy for turbidity because differences in water content will be a main contributor to the refractive index contrast between supernatant and coacervate phases. We can use this quantity to show that our results are indeed consistent with experimental observations. For our calculations, an excess of one of the two salt ions is added to render the system electroneutral, while at the same time ensuring that the charge fractions $\langle f_{d,\pm}\rangle$ of both chains are consistent. We plot in Figure 8b the concentration of the salt species as a function of Θ_+. $\Delta\phi_W$ verus Θ_+ is shown in Figure 8a for a number of different pH values, with a focus on the same pH values as in Figure 5. We observe a maximum in the disparity $\Delta\phi_W$ at $\Theta_+ = 0.5$ for a pH of 7, which is expected when both polymers are symmetrically, fully charged. However, as pH decreases and $\langle f_{d,P-}\rangle < 1$, the peak of maximum $\Delta\phi_W$ shifts to lower values of Θ_+. This is consistent with the previous phase diagrams, where the peak value of $\Theta_+ \approx 0.35$ for pH = 2.6, but also consistent with experiments by Perry et al.[1]

CONCLUSION

We have extended the transfer matrix formalism for complex coacervation to account for pH effects. This is done by explicitly accounting for the energetic cost and benefit of forming a variety of ion pairs between a polyelectrolyte and surrounding salt and oppositely charged polyelectrolyte species, and allowing for both charged and uncharged monomer states. This formalism allows access to both the interaction free energy of the polyelectrolyte with its surroundings, as well as its charge fraction; this latter property has the Henderson-Hasselbalch as its limiting case, directly connecting this formalism to classical theories of weak electrolytes.

Considering the pK_a for a pair of polyelectrolytes, poly(aspartate) and poly(lysine), we show that there is a broad pH window in which both the polycation and polyanion are fully charged, but at high or low pH we observe a transition to one of the polyelectrolyte species being uncharged. The window where both species are fully charged is dependent on the environment, with the repulsion between adjacent monomer charges shrinking this window and suppressing polyelectrolyte charging, while the presence of salt and polyelectrolytes of opposite charge can facilitate charging. Indeed, the primary effect in coacervates is predicted to be the cooperative charging of both polycation and polyanion, as the dissociation is favored by the presence of nearby charges of the opposite sign.

With this insight, we are able to demonstrate phase behavior in weak polyelectrolyte coacervation, which we do so by focusing on the dissociation transition at low pH for the polyanion. The main physical effects are 2-fold; first, the weakly charged polyanion in the coacervate phase means that anions must be recruited so that this phase is electroneutral, thus depleting the anion species in the supernatant and decreasing the size of the two-phase region of the phase diagram. The second effect is that the low polyelectrolyte and salt concentration in the supernatant leads to less dissociation of the polyanion species in that phase, though this effect weakens with increasing salt concentration.

We also explored the phase behavior of nonstoichiometric mixtures of polyelectrolytes, which also exhibit "shifted" phase diagrams between positively and negatively charged species as more of one of the salt species is needed to maintain electroneutrality. Near the $pK_{a,eff}$ of polyanions ($\approx$ 2.5 in coacervates), an abundance of partially charged polyanions is needed to neutralize fully charged polycations, such that a polycation fraction $\Theta_+ \approx 0.35$ exhibits optimal coacervation behavior (i.e., a large two-phase region). This occurs because when the two polyelectrolyte species are in charge balance, the system does not need to maintain an excess of small molecular charges in the coacervate. The region of coacervation begins to shrink as Θ_+ deviates form this optimal value.

Our method for capturing pH effects in coacervates relies on a number of parameters, which we do not tune here to reflect any specific experimental system. However, given a clear physical interpretation of, for example, Γ_0, Γ_1, etc., it should be straightforward to parametrize these aspects of the model to account for behaviors seen in experiment. The partitioning of salt ions represents a feasible route to testing these predictions,[100,101] as we expect significant differences between the two salt ions in both phases. There have been some initial effort in the literature to do this,[89] though nonelectrostatic interactions complicate comparison with theoretical models. Simulation would also be an effective way to assess these physical predictions,[88,140,160] and would be able to directly test key approximations made in the transfer matrix formalism.[129] In particular, the assumption of a mean-field environment of positive and negative charges around the test chain in our formalism is likely not accurate at low polymer concentrations seen in the dilute phase. Further insight from both experimental and computational efforts will be crucial for continued development of our understanding of weak-polyelectrolyte coacervates.

https://doi.org/10.1021/acs.jpcb.1c03065
J. Phys. Chem. B 2021, 125, 8965−8980

AUTHOR INFORMATION

Corresponding Author

Charles E. Sing − *Department of Chemical and Biomolecular Engineering, University of Illinois at Urbana−Champaign, Urbana, Illinois 61801, United States;* orcid.org/0000-0001-7231-2685; Email: cesing@illinois.edu

Authors

Ashley R. Knoerdel − *Program in Biophysics and Quantitative Biology, University of Illinois at Urbana−Champaign, Urbana, Illinois 61801, United States*

Whitney C. Blocher McTigue − *Department of Chemical and Biomolecular Engineering, University of Illinois at Urbana−Champaign, Urbana, Illinois 61801, United States*

Complete contact information is available at: https://pubs.acs.org/10.1021/acs.jpcb.1c03065

Notes

The authors declare no competing financial interest.

ACKNOWLEDGMENTS

The authors acknowledge support by the National Science Foundation under Grant No. DMR-1654158.

REFERENCES

(1) Perry, S. L.; Li, Y.; Priftis, D.; Leon, L.; Tirrell, M. The effect of salt on the complex coacervation of vinyl polyelectrolytes. *Polymers* **2014**, *6*, 1756−1772.

(2) Priftis, D.; Leon, L.; Song, Z.; Perry, S.; Margossian, K.; Tropnikova, A.; Cheng, J.; Tirrell, M. Self-Assembly of α-Helical Polypeptides Driven by Complex Coacervation. *Angew. Chem., Int. Ed.* **2015**, *54*, 11128−11132.

(3) Hoffmann, K. Q.; Perry, S. L.; Leon, L.; Priftis, D.; Tirrell, M.; de Pablo, J. J. A Molecular View of the Role of Chirality in Charge-Driven Polypeptide Complexation. *Soft Matter* **2015**, *11*, 1525−1538.

(4) Perry, S. L.; Leon, L.; Hoffmann, K. Q.; Kade, M. J.; Priftis, D.; Black, K. A.; Wong, D.; Klein, R. A.; III, C. F. P.; Margossian, K. O.; et al. Chirality-selected phase behaviour in ionic polypeptide complexes. *Nat. Commun.* **2015**, *6*, 6052.

(5) Black, K. A.; Priftis, D.; Perry, S. L.; Yip, J.; Byun, W. Y.; Tirrell, M. Protein encapsulation via polypeptide complex coacervation. *ACS Macro Lett.* **2014**, *3*, 1088−1091.

(6) Obermeyer, A.; Mills, C.; Dong, X.; Flores, R.; Olsen, B. Complex coacervation of supercharged proteins with polyelectrolytes. *Soft Matter* **2016**, *12*, 3570−3581.

(7) Pippa, N.; Karayianni, M.; Pispas, S.; Demetzos, C. Complexation of cationic-neutral block polyelectrolyte with insulin and in vitro release studies. *Int. J. Pharm.* **2015**, *491*, 136−143.

(8) Pippa, N.; Kalinova, R.; Dimitrov, I.; Pispas, S.; Demetzos, C. Insulin/poly(ethylene glycol)- block-poly(l-lysine) Complexes: Physicochemical Properties and Protein Encapsulation. *J. Phys. Chem. B* **2015**, *119*, 6813−6819.

(9) Nolles, A.; Westphal, A.; de Hoop, J.; Fokkink, R.; Kleijn, J.; van Berkel, W.; Borst, J. Encapsulation of GFP in Complex Coacervate Core Micelles. *Biomacromolecules* **2015**, *16*, 1542−1549.

(10) Mi, X.; Blocher McTigue, W. C.; Joshi, P. U.; Bunker, M. K.; Heldt, C. L.; Perry, S. L. Thermostabilization of Viruses via Complex Coacervation. *Biomater. Sci.* **2020**, *8*, 7082−7092.

(11) Chen, W. C. W.; Lee, B. G.; Park, D. W.; Kim, K.; Chu, H.; Kim, K.; Huard, J.; Wang, Y. Controlled dual delivery of fibroblast growth factor-2 and Interleukin-10 by heparin-based coacervate synergistically enhances ischemic heart repair. *Biomaterials* **2015**, *72*, 138−151.

(12) Kim, S.; Huang, J.; Lee, Y.; Dutta, S.; Yoo, H. Y.; Jung, Y. M.; Jho, Y.; Zeng, H.; Hwang, D. S. Complexation and coacervation of like-charged polyelectrolytes inspired by mussels. *Proc. Natl. Acad. Sci. U. S. A.* **2016**, *113*, E847−E853.

(13) Kawamura, A.; Harada, A.; Kono, K.; Kataoka, K. Self-Assembled Nano-Bioreactor from Block Ionomers with Elevated and Stabilized Enzymatic Function. *Bioconjugate Chem.* **2007**, *18*, 1555−1559.

(14) Jaturanpinyo, M.; Harada, A.; Yuan, X.; Kataoka, K. Preparation of Bionanoreactor Based on Core-Shell Structured Polyion Complex Micelles Entrapping Trypsin in the Core Cross-Linked with Glutaraldehyde. *Bioconjugate Chem.* **2004**, *15*, 344−348.

(15) Harada, A.; Kataoka, K. Formation of polyion complex micelles in an aqueous milieu from a pair of oppositely-charged block copolymers with poly(ethylene glycol) segments. *Macromolecules* **1995**, *28*, 5294−5299.

(16) Harada, A.; Kataoka, K. Pronounced activity of enzymes through the incorporation into the core of polyion complex micelles made from charged block copolymers. *J. Controlled Release* **2001**, *72*, 85−91.

(17) Kataoka, K.; Harada, A.; Nagasaki, Y. Block copolymer micelles for drug delivery: design, characterization and biological significance. *Adv. Drug Delivery Rev.* **2001**, *47*, 113−131.

(18) Harada, A.; Kataoka, K. Novel Polyion Complex Micelles Entrapping Enzyme Molecules in the Core: Preparation of Narrowly-Distributed Micelles from Lysozyme and Poly(ethylene glycol)-Poly(aspartic acid) Block Copolymer in Aqueous Medium. *Macromolecules* **1998**, *31*, 288−294.

(19) Yan, Y.; Kizilay, E.; Seeman, D.; Flanagan, S.; Dubin, P. L.; Bovetto, L.; Donato, L.; Schmitt, C. Heteroprotein complex coacervation: bovine β-lactoglobulin and lactoferrin. *Langmuir* **2013**, *29*, 15614−15623.

(20) Kayitmazer, A. B.; Seeman, D.; Minsky, B. B.; Dubin, P. L.; Xu, Y. Protein-polyelectrolyte interactions. *Soft Matter* **2013**, *9*, 2553−2583.

(21) Antonov, M.; Mazzawi, M.; Dubin, P. L. Entering and Exiting the Protein-Polyelectrolyte Coacervate Phase via Nonmonotonic Salt Dependence of Critical Conditions. *Biomacromolecules* **2010**, *11*, 51−59.

(22) Kapelner, R. A.; Obermeyer, A. C. Ionic polypeptide tags for protein phase separation. *Chem. Sci.* **2019**, *9*, No. e1442.

(23) Kayitmazer, A. B.; Seyrek, E.; Dubin, P. L.; Staggemeier, B. A. Influence of Chain Stiffness on the Interaction of Polyelectrolytes with Oppositely Charged Micelles and Proteins. *J. Phys. Chem. B* **2003**, *107*, 8158−8165.

(24) Kalantar, T. H.; Tucker, C. J.; Zalusky, A. S.; Boomgaard, T. A.; Wilson, B. E.; Ladika, M.; Jordan, S. L.; Li, W. K.; Zhang, X.; Goh, C. G. High throughput workflow for coacervate formation and characterization in shampoo systems. *J. Cosmetic Sci.* **2007**, *58*, 375−383.

(25) Hu, D.; Chou, K. C. Re-evaluating the surface tension analysis of polyelectrolyte-surfactant mixtures using phase-sensitive sum frequency generation spectroscopy. *J. Am. Chem. Soc.* **2014**, *136*, 15114−15117.

(26) Nejati, M. M.; Khaledi, M. G. Perfluoro-alcohol-induced complex coacervates of polyelectrolyte−surfactant mixtures: Phase behavior and analysis. *Langmuir* **2015**, *31*, 5580−5589.

(27) Wang, Y.; Kimura, K.; Huang, Q.; Dubin, P. L.; Jaeger, W. Effects of Salt on Polyelectrolyte-Micelle Coacervation. *Macromolecules* **1999**, *32*, 7128−7134.

(28) Wang, W.; Mauroy, H.; Zhu, K.; Knudsen, K. D.; Kjøniksen, A.-L.; Nyström, B.; Sande, S. A. Complex coacervate micelles formed by a C18-capped cationic triblock thermoresponsive copolymer interacting with SDS. *Soft Matter* **2012**, *8*, 11514−11525.

(29) Kizilay, E.; Kayitmazer, A. B.; Dubin, P. L. Complexation and coacervation of polyelectrolytes with oppositely charged colloids. *Adv. Colloid Interface Sci.* **2011**, *167*, 24−37.

(30) Turgeon, S. L.; Schmitt, C.; Sanchez, C. Protein-polysaccharide complexes and coacervates. *Curr. Opin. Colloid Interface Sci.* **2007**, *12*, 166−178.

(31) Schmitt, C.; Turgeon, S. L. Protein/polysaccharide complexes and coacervates in food systems. *Adv. Colloid Interface Sci.* **2011**, *167*, 63−70.

(32) Matalanis, A.; Jones, O. G.; McClements, D. J. Food Hydrocolloids. Structured biopolymer-based delivery systems for encapsulation, protection. *Food Hydrocolloids* **2011**, *25*, 1865−1880.

(33) Weinbreck, F.; de Vries, R.; Schrooyen, P.; de Kruif, C. G. Complex coacervation of whey proteins and gum arabic. *Biomacromolecules* **2003**, *4*, 293−303.
(34) Yeo, Y.; Bellas, E.; Firestone, W.; Langer, R.; Kohane, D. S. Complex Coacervates for Thermally Sensitive Controlled Release of Flavor Compounds. *J. Agric. Food Chem.* **2005**, *53*, 7518−7525.
(35) Jourdain, L.; Leser, M. E.; Schmitt, C.; Michel, M.; Dickinson, E. Stability of emulsions containing sodium caseinate and dextran sulfate: Relationship to complexation in solution. *Food Hydrocolloids* **2008**, *22*, 647−659.
(36) Hwang, D. S.; Zeng, H.; Srivastava, A.; Krogstad, D. V.; Tirrell, M.; Israelachvili, J. N.; Waite, J. Viscosity and interfacial properties in a mussel-inspired adhesive coacervate. *Soft Matter* **2010**, *6*, 3232−3236.
(37) Ahn, B. K.; Das, S.; Linstadt, R.; Kaufman, Y.; Martinez-Rodriguez, N. R.; Mirshafian, R.; Kesselman, E.; Talmon, Y.; Lipshutz, B. H.; Israelachvili, J. N.; Waite, J. H. High-performance mussel-inspired adhesives of reduced complexity. *Nat. Commun.* **2015**, *6*, 8663.
(38) Stewart, R. J.; Wang, C. S.; Shao, H. Complex coacervates as a foundation for synthetic underwater adhesives. *Adv. Colloid Interface Sci.* **2011**, *167*, 85−93.
(39) Lim, S.; Moon, D.; Kim, H. J.; Seo, S. H.; Kang, I. S.; Cha, H. J. Interfacial tension of complex coacervated mussel adhesive protein according to the Hofmeister series. *Langmuir* **2014**, *30*, 1108−1115.
(40) Wang, W.; Xu, Y.; Li, A.; Li, T.; Liu, M.; von Klitzing, R.; Ober, C. K.; Kayitmazer, A. B.; Li, L.; Guo, X. Zinc induced polyelectrolyte coacervate bioadhesive and its transition to a self-healing hydrogel. *RSC Adv.* **2015**, *5*, 66871−66878.
(41) Winslow, B. D.; Shao, H.; Stewart, R. J.; Tresco, P. A. Biocompatibility of adhesive complex coacervates modeled after the sandcastle glue of Phragmatopoma californica for craniofacial reconstruction. *Biomaterials* **2010**, *31*, 9373−9381.
(42) Mann, L. K.; Papanna, R.; Moise, K. J., Jr; Byrd, R. H.; Popek, E. J.; Kaur, S.; Tseng, S. C. G.; Stewart, R. J. Fetal membrane patch and biomimetic adhesive coacervates as a sealant for fetoscopic defects. *Acta Biomater.* **2012**, *8*, 2160−2165.
(43) Lim, S.; Choi, Y. S.; Kang, D. G.; Song, Y. H.; Cha, H. J. The adhesive properties of coacervated recombinant hybrid mussel adhesive proteins. *Biomaterials* **2010**, *31*, 3715−3722.
(44) Hwang, D. S.; Zeng, H.; Lu, Q.; Israelachvili, J.; Waite, J. H. Adhesion mechanism in a DOPA-deficient foot protein from green mussels. *Soft Matter* **2012**, *8*, 5640−9.
(45) Kaur, S.; Weerasekare, G. M.; Stewart, R. J. Multiphase Adhesive Coacervates Inspired by the Sandcastle Worm. *ACS Appl. Mater. Interfaces* **2011**, *3*, 941−944.
(46) Choi, Y. S.; Kang, D. G.; Lim, S.; Yang, Y. J.; Kim, C. S.; Cha, H. J. Recombinant mussel adhesive protein fp-5 (MAP fp-5) as a bulk bioadhesive and surface coating material. *Biofouling* **2011**, *27*, 729−737.
(47) Shao, H.; Weerasekare, G. M.; Stewart, R. J. Controlled curing of adhesive complex coacervates with reversible periodate carbohydrate complexes. *J. Biomed. Mater. Res., Part A* **2011**, *97A*, 46−51.
(48) Shao, H.; Bachus, K. N.; Stewart, R. J. A Water-Borne Adhesive Modeled after the Sandcastle Glue of P. californica. *Macromol. Biosci.* **2009**, *9*, 464−471.
(49) Lindhoud, S.; de Vries, R.; Schweins, R.; Cohen Stuart, M.; Norde, W. Salt-induced release of lipase from polyelectrolyte complex micelles. *Soft Matter* **2009**, *5*, 242−250.
(50) Lindhoud, S.; de Vries, R.; Schweins, R.; Cohen Stuart, M.; Norde, W. Structure and Stability of Complex Coacervate Core Micelles with Lysozyme. *Biomacromolecules* **2007**, *8*, 2219−2227.
(51) Lindhoud, S.; Claessens, M. Accumulation of small protein molecules in a macroscopic complex coacervate. *Soft Matter* **2016**, *12*, 408−413.
(52) Kishimura, A.; Koide, A.; Osada, K.; Yamasaki, Y.; Kataoka, K. Encapsulation of Myoglobin in PEGylated Polyion Complex Vesicles Made from a Pair of Oppositely Charged Block Ionomers: A Physiologically Available Oxygen Carrier. *Angew. Chem., Int. Ed.* **2007**, *46*, 6085−6088.
(53) Chu, H.; Gao, J.; Chen, C. W.; Huard, J.; Wang, Y. Injectable fibroblast growth factor-2 coacervate for persistent angiogenesis. *Proc. Natl. Acad. Sci. U. S. A.* **2011**, *108*, 13444−13449.
(54) Aumiller, W. M.; Keating, C. D. Phosphorylation-mediated RNA/peptide complex coacervation as a model for intracellular liquid organelles. *Nat. Chem.* **2016**, *8*, 129−137.
(55) Cabral, H.; Miyata, K.; Osada, K.; Kataoka, K. Block Copolymer Micelles in Nanomedicine Applications. *Chem. Rev.* **2018**, *118*, 6844−6892.
(56) Chida, T.; Miura, Y.; Cabral, H.; Nomoto, T.; Kataoka, K.; Nishiyama, N. Epirubicin-loaded polymeric micelles effectively treat axillary lymph nodes metastasis of breast cancer through selective accumulation and pH-triggered drug release. *J. Controlled Release* **2018**, *292*, 130−140.
(57) Frankel, E. A.; Bevilacqua, P. C.; Keating, C. D. Polyamine/Nucleotide coacervates provide strong compartmentalization of Mg 2+, nucleotides, and RNA. *Langmuir* **2016**, *32*, 2041−2049.
(58) Tang, T. Y. D.; Antognozzi, M.; Vicary, J. A.; Perriman, A. W.; Mann, S. Small-molecule uptake in membrane-free peptide/nucleotide protocells. *Soft Matter* **2013**, *9*, 7647−7656.
(59) Arfin, N.; Aswal, V. K.; Bohidar, H. B. Overcharging, thermal, viscoelastic and hydration properties of DNA−gelatin complex coacervates: pharmaceutical and food industries. *RSC Adv.* **2014**, *4*, 11705−9.
(60) Perry, S. L.; Neumann, S. G.; Neumann, T.; Cheng, K.; Ni, J.; Weinstein, J. R.; Schaffer, D. V.; Tirrell, M. Challenges in nucleic acid-lipid films for transfection. *AIChE J.* **2013**, *59*, 3203−3213.
(61) Kinoh, H.; Miura, Y.; Chida, T.; Liu, X.; Mizuno, K.; Fukushima, S.; Morodomi, Y.; Nishiyama, N.; Cabral, H.; Kataoka, K. Nanomedicines eradicating cancer stem-like cells in vivo by pH-triggered intracellular cooperative action of loaded drugs. *ACS Nano* **2016**, *10*, 5643−5655.
(62) Yen, J.; Ying, H.; Wang, H.; Yin, L.; Uckun, F.; Cheng, J. CD44 mediated nonviral gene delivery into human embryonic stem cells via hyaluronic-acid-coated nanoparticles. *ACS Biomater. Sci. Eng.* **2016**, *2*, 326−335.
(63) Chu, H.; Chen, C.-W.; Huard, J.; Wang, Y. The effect of a heparin-based coacervate of fibroblast growth factor-2 on scarring in the infarcted myocardium. *Biomaterials* **2013**, *34*, 1747−1756.
(64) Kuo, C.-H.; Leon, L.; Chung, E. J.; Huang, R.-T.; Sontag, T. J.; Reardon, C. A.; Getz, G. S.; Tirrell, M.; Fang, Y. Inhibition of atherosclerosis-promoting microRNAs via targeted polyelectrolyte complex micelles. *J. Mater. Chem. B* **2014**, *2*, 8142−8153.
(65) Jin, K.-M.; Kim, Y.-H. Injectable, thermo-reversible and complex coacervate combination gels for protein drug delivery. *J. Controlled Release* **2008**, *127*, 249−256.
(66) Anraku, Y.; Kishimura, A.; Kamiya, M.; Tanaka, S.; Nomoto, T.; Toh, K.; Matsumoto, Y.; Fukushima, S.; Sueyoshi, D.; Kano, M. R.; et al. Systemically injectable enzyme-loaded polyion complex vesicles as in vivo nanoreactors functioning in tumors. *Angew. Chem.* **2016**, *128*, 570−575.
(67) Schoonen, L.; van Hest, J. C. M. Compartmentalization approaches in soft matter science: From nanoreactor development to organelle mimics. *Adv. Mater.* **2016**, *28*, 1109−1128.
(68) Lv, K.; Perriman, A. W.; Mann, S. Photocatalytic multiphase micro-droplet reactors based on complex coacervation. *Chem. Commun.* **2015**, *51*, 8600−8602.
(69) Hyman, A. A.; Simons, K. Beyond oil and water - phase transitions in cells. *Science* **2012**, *337*, 1047−1049.
(70) Weber, S. C.; Brangwynne, C. P. Getting RNA and protein in phase. *Cell* **2012**, *149*, 1188−1191.
(71) Elbaum-Garfinkle, S.; Kim, Y.; Szczepaniak, K.; Chen, C. C.-H.; Eckmann, C. R.; Myong, S.; Brangwynne, C. P. The disordered P granule protein LAF-1 drives phase separation into droplets with tunable viscosity and dynamics. *Proc. Natl. Acad. Sci. U. S. A.* **2015**, *112*, 7189−7194.
(72) Brangwynne, C. P.; Mitchison, T. J.; Hyman, A. A. Active liquid-like behavior of nucleoli determines their size and shape in Xenopus laevis oocytes. *Proc. Natl. Acad. Sci. U. S. A.* **2011**, *108*, 4334−4339.

https://doi.org/10.1021/acs.jpcb.1c03065
J. Phys. Chem. B 2021, 125, 8965−8980

(73) Brangwynne, C. P.; Eckmann, C.; Courson, D.; Rybarska, A.; Hoege, C.; Gharakhani, J.; Jülicher, F.; Hyman, A. A. Germline P granules are liquid droplets that localize by controlled dissolution/condensation. *Science* **2009**, *324*, 1729−1732.
(74) Hyman, A. A.; Brangwynne, C. P. Beyond Stereospecificity: Liquids and Mesoscale Organization of Cytoplasm. *Dev. Cell* **2011**, *21*, 14−16.
(75) Kato, M.; Han, T. W.; Xie, S.; Shi, K.; Du, X.; Wu, L. C.; Mirzaei, H.; Goldsmith, E. J.; Longgood, J.; Pei, J.; et al. Cell-free Formation of RNA Granules: Low Complexity Sequence Domains Form Dynamic Fibers within Hydrogels. *Cell* **2012**, *149*, 753−767.
(76) Eulalio, A.; Behm-Ansmant, I.; Izaurralde, E. P bodies: at the crossroads of post-transcriptional pathways. *Nat. Rev. Mol. Cell Biol.* **2007**, *8*, 9−22.
(77) Han, T. W.; Kato, M.; Xie, S.; Wu, L. C.; Mirzaei, H.; Pei, J.; Chen, M.; Xie, Y.; Allen, J.; Xiao, G.; et al. Cell-free Formation of RNA Granules: Bound RNAs Identify Features and Components of Cellular Assemblies. *Cell* **2012**, *149*, 768−779.
(78) Jia, T. Z.; Hentrich, C.; Szostak, J. W. Rapid RNA exchange in aqueous two-phase system and coacervate droplets. *Origins Life Evol. Biospheres* **2014**, *44*, 1−12.
(79) Li, P.; Banjade, S.; Cheng, H.-C.; Kim, S.; Chen, B.; Guo, L.; Llaguno, M.; Hollingsworth, J. V.; King, D. S.; Banani, S. F.; et al. Phase transitions in the assembly of multivalent signalling proteins. *Nature* **2012**, *483*, 336−340.
(80) Zhang, H.; Elbaum-Garfinkle, S.; Langdon, E. M.; Taylor, N.; Occhipinti, P.; Bridges, A. A.; Brangwynne, C. P.; Gladfelter, A. S. RNA controls PolyQ protein phase transitions. *Mol. Cell* **2015**, *60*, 220−230.
(81) Lin, Y.; Protter, D. S. W.; Rosen, M. K.; Parker, R. Formation and maturation of phase-separated liquid droplets by RNA-binding proteins. *Mol. Cell* **2015**, *60*, 208−219.
(82) Fromm, S.; Kamenz, J.; Nöldeke, E.; Neu, A.; Zocher, G.; Sprangers, R. In vitro reconstitution of a cellular phase-transition process that involves the mRNA decapping machinery. *Angew. Chem., Int. Ed.* **2014**, *53*, 7354−7359.
(83) Patel, A.; Lee, H. O.; Jawerth, L.; Maharana, S.; Jahnel, M.; Hein, M. Y.; Stoynov, S.; Mahamid, J.; Saha, S.; Franzmann, T. M.; et al. A liquid-to-solid phase transition of the ALS protein FUS accelerated by disease mutation. *Cell* **2015**, *162*, 1066−1077.
(84) Burke, K. A.; Janke, A. M.; Rhine, C. L.; Fawzi, N. L. Residue-by-residue view of in vitro FUS granules that bind the C-terminal domain of RNA polymerase II. *Mol. Cell* **2015**, *60*, 231−241.
(85) Water, J. J.; Schack, M. M.; Velazquez-Campoy, A.; Maltesen, M. J.; van de Weert, M.; Jorgensen, L. Complex coacervates of hyaluronic acid and lysozyme: Effect on protein structure and physical stability. *Eur. J. Pharm. Biopharm.* **2014**, *88*, 325−331.
(86) Blocher McTigue, W.; Perry, S. Design rules for encapsulating proteins into complex coacervates. *Soft Matter* **2019**, *15*, 3089−3103.
(87) Priftis, D.; Tirrell, M. Phase behaviour and complex coacervation of aqueous polypeptide solutions. *Soft Matter* **2012**, *8*, 9396−9405.
(88) Rathee, V. S.; Zervoudakis, A. J.; Sidky, H.; Sikora, B. J.; Whitmer, J. K. Weak polyelectrolyte complexation driven by associative charging. *J. Chem. Phys.* **2018**, *148*, 114901.
(89) Li, L.; Srivastava, S.; Meng, S.; Ting, J.; Tirrell, M. Effects of non-electrostatic intermolecular interactions on the phase behavior of pH-sensitive polyelectrolyte complexes. *Macromolecules* **2020**, *53*, 7835−7844.
(90) Spruijt, E.; Westphal, A. H.; Borst, J. W.; Cohen Stuart, M. A.; van der Gucht, J. Binodal compositions of polyelectrolyte complexes. *Macromolecules* **2010**, *43*, 6476−6484.
(91) Marciel, A. B.; Srivastava, S.; Tirrell, M. V. Structure and rheology of polyelectrolyte complex coacervates. *Soft Matter* **2018**, *14*, 2454.
(92) Vieregg, J. R.; Lueckheide, M.; Marciel, A. B.; Leon, L.; Bologna, A. J.; Rivera, J. R.; Tirrell, M. V. Oligonucleotide-peptide complexes: Phase control by hybridization. *J. Am. Chem. Soc.* **2018**, *140*, 1632−1638.
(93) Chang, L. W.; Lytle, T. K.; Radhakrishna, M.; Madinya, J. J.; Vélez, J.; Sing, C. E.; Perry, S. L. Sequence and entropy-based control of complex coacervates. *Nat. Commun.* **2017**, *8*, 1273.
(94) Johnston, B. M.; Johnston, C. W.; Letteri, R. A.; Lytle, T. K.; Sing, C. E.; Emrick, T.; Perry, S. L. The effect of comb architecture on complex coacervation. *Org. Biomol. Chem.* **2017**, *15*, 7630−7642.
(95) Zhang, P.; Alsaifi, N. M.; Wu, J.; Wang, Z.-G. Polyelectrolyte complex coacervation: Effects of concentration asymmetry. *J. Chem. Phys.* **2018**, *149*, 163303.
(96) Liu, Y.; Winter, H. H.; Perry, S. L. Linear viscoelasticity of complex coacervates. *Adv. Colloid Interface Sci.* **2017**, *239*, 46.
(97) Liu, Y.; B, M.; Winter, H.; Perry, S. Rheological characterization of liquid-to-solid transitions in bulk polyelectrolyte complexes. *Soft Matter* **2017**, *13*, 7332−7340.
(98) Tekaat, M.; Bütergerds, D.; Schönhoff, M.; Fery, A.; Cramer, C. Scaling properties of the shear modulus of polyelectrolyte complex coacervates: a time-pH superposition principle. *Phys. Chem. Chem. Phys.* **2015**, *17*, 22552−22556.
(99) Raei, M.; Rafe, A.; Shahidi, F. Rheological and structural characteristics of whey protein-pectin complex coacervates. *J. Food Eng.* **2018**, *228*, 25−31.
(100) Radhakrishna, M.; Basu, K.; Liu, Y.; Shamsi, R.; Perry, S. L.; Sing, C. E. Molecular Connectivity and Correlation Effects on Polymer Coacervation. *Macromolecules* **2017**, *50*, 3030−3037.
(101) Li, L.; Srivastava, S.; Andreev, M.; Marciel, A. B.; de Pablo, J. J.; Tirrell, M. V. Phase behavior and salt partitioning in polyelectrolyte complex coacervates. *Macromolecules* **2018**, *51*, 2988−2995.
(102) Li, L.; Rumyantsev, A.; Srivastava, S.; Meng, S.; de Pablo, J.; Tirrell, M. Effect of solvent quality on the phase behavior of polyelectrolyte complexes. *Macromolecules* **2021**, *54*, 105−114.
(103) Michaeli, I.; Overbeek, J. T. G.; Voorn, M. Phase separation of polyelectrolyte solutions. *J. Polym. Sci.* **1957**, *23*, 443−450.
(104) Overbeek, J. T. G.; Voorn, M. Phase separation in polyelectrolyte solutions. Theory of complex coacervation. *J. Cell. Comp. Physiol.* **1957**, *49*, 7−26.
(105) Flory, P. J. *Principles of Polymer Chemistry*; Cornell University Press: Ithaca, NY, 1953.
(106) Debye, P.; Huckel, E. Theory of electrolytes. *Phys. Z.* **1923**, *24*, 185.
(107) McQuarrie, D. A. *Statistical Mechanics*; University Science Books: Sausalito, 2000.
(108) Sing, C. E. Development of the modern theory of polymeric complex coacervation. *Adv. Colloid Interface Sci.* **2017**, *239*, 2−16.
(109) Perry, S. L.; Sing, C. E. Prism-based theory of complex coacervation: Excluded volume versus chain correlation. *Macromolecules* **2015**, *48*, 5040−5053.
(110) Borue, V. Y.; Erukhimovich, I. Y. A statistical theory of globular polyelectrolyte complexes. *Macromolecules* **1990**, *23*, 3625−3632.
(111) Castelnovo, M.; Joanny, J.-F. Complexation between oppositely charged polyelectrolytes: Beyond the Random Phase Approximation. *Eur. Phys. J. E: Soft Matter Biol. Phys.* **2001**, *6*, 377−386.
(112) Kudlay, A.; Ermoshkin, A. V.; Cruz, M. O. d. l. Comoplexation of oppositely charged polyelectrolytes: effect of ion pair formation. *Macromolecules* **2004**, *37*, 9231−9241.
(113) Kudlay, A.; Olvera de la Cruz, M. Precipitation of oppositely charged polyelectrolytes in salt solutions. *J. Chem. Phys.* **2004**, *120*, 404−412.
(114) Qin, J.; de Pablo, J. J. Criticality and connectivity in macromolecular charge complexation. *Macromolecules* **2016**, *49*, 8789−8800.
(115) Lee, J.; Popov, Y. O.; Fredrickson, G. H. Complex coacervation: A field theoretic simulation study of polyelectrolyte complexation. *J. Chem. Phys.* **2008**, *128*, 224908.
(116) Riggleman, R. A.; Kumar, R.; Fredrickson, G. H. Investigation of the interfacial tension of complex coacervates using field-theoretic simulations. *J. Chem. Phys.* **2012**, *136*, 024903.
(117) Delaney, K. T.; Fredrickson, G. H. Theory of polyelectrolyte complexation - Complex coacervates are self-coacervates. *J. Chem. Phys.* **2017**, *146*, 224902.
(118) Danielsen, S. P. O.; McCarty, J.; Shea, J.-E.; Delaney, K. T.; Fredrickson, G. H. Molecular design of self-coacervation phenomena in

https://doi.org/10.1021/acs.jpcb.1c03065
J. Phys. Chem. B 2021, 125, 8965−8980

block polyampholytes. *Proc. Natl. Acad. Sci. U. S. A.* **2019**, *116*, 8224−8232.
(119) Danielsen, S. P. O.; McCarty, J.; Shea, J.-E.; Delaney, K.; Fredrickson, G. Small ion effects on self-coacervation phenomena in block polyampholytes. *J. Chem. Phys.* **2019**, *151*, 034904.
(120) Shusharina, N.; Zhulina, E.; Dobrynin, A.; Rubinstein, M. Scaling theory of diblock polyampholyte solutions. *Macromolecules* **2005**, *38*, 8870−8881.
(121) Wang, Z.; Rubinstein, M. Regimes of conformational transitions of a diblock polyampolyte. *Macromolecules* **2006**, *39*, 5897−5912.
(122) Rubinstein, M.; Liao, Q.; Panyukov, S. Structure of Liquid Coacervates Formed by Oppositely Charged Polyelectrolytes. *Macromolecules* **2018**, *51*, 9572−9588.
(123) Rumyantsev, A. M.; Zhulina, E. B.; Borisov, O. V. Complex coacervate of weakly charged chains: Diagram of states. *Macromolecules* **2018**, *51*, 3788−3801.
(124) Rumyantsev, A. M.; de Pablo, J. J. Liquid crystalline and isotropic coacervates of semiflexible polyanions and flexible polycations. *Macromolecules* **2019**, *52*, 5140−5156.
(125) Rumyantsev, A. M.; Kramarenko, E. Y.; Borisov, O. V. Microphase separation in complex coacervate due to incompatibility between polyanion and polycation. *Macromolecules* **2018**, *51*, 6587−6601.
(126) Zhang, P.; Shen, K.; Alsaifi, N. M.; Wang, Z.-G. Salt partitioning in complex coacervation of symmetric polyelectrolytes. *Macromolecules* **2018**, *51*, 5586−5593.
(127) Sing, C.; Perry, S. Recent progress in the science of complex coacervation. *Soft Matter* **2020**, *16*, 2885.
(128) Andreev, M.; Prabhu, V. M.; Douglas, J. F.; Tirrell, M. V.; de Pablo, J. J. Complex coacervation in polyelectrolytes from a coarse-grained model. *Macromolecules* **2018**, *51*, 6717−6723.
(129) Lytle, T. K.; Salazar, A. J.; Sing, C. E. Interfacial properties of polymeric complex coacervates from simulation and theory. *J. Chem. Phys.* **2018**, *149*, 163315.
(130) Lytle, T. K.; Chang, L.-W.; Markiewicz, N.; Perry, S. L.; Sing, C. E. Designing Electrostatic Interactions via Polyelectrolyte Monomer Sequence. *ACS Cent. Sci.* **2019**, *5*, 709−718.
(131) Mintis, D.; Mavrantzas, V. Phase boundary and salt partitioning in coacervate complexes formed between poly(acrylic acid) and poly(n,n-dimethylaminoethyl methacrylate) from detailed atomistic simulations combined with free energy perturbation and thermodynamic integration calculations. *Macromolecules* **2020**, *53*, 7618.
(132) Blocher, W.; Perry, S. Complex coacervate-based materials for biomedicine. *WIREs Nanomed. Nanobiotech.* **2017**, *9*, No. e1442.
(133) Lindhoud, S.; Voorhaar, L.; de Vries, R.; Schweins, R.; Cohen Stuart, M.; Norde, W. Salt-Induced Disintegration of Lysozyme-Containing Polyelectrolyte Complex Micelles. *Langmuir* **2009**, *25*, 11425−11430.
(134) Cummings, C. S.; Obermeyer, A. C. Phase separation behavior of supercharged proteins and polyelectrolytes. *Biochemistry* **2018**, *57*, 314−323.
(135) Cakmak, F.; Choi, S.; Meyer, M.; Bevilacqua, P.; Keating, C. Prebiotically-relevant low polyion multivalency can improve functionality of membraneless compartments. *Nat. Commun.* **2020**, *11*, 5949.
(136) Meng, X.; Perry, S.; Schiffman, J. Complex Coacervation: Chemically Stable Fibers Electrospun from Aqueous Polyelectrolyte Solutions. *ACS Macro Lett.* **2017**, *6*, 505−511.
(137) Dickhaus, B. N.; Priefer, R. Determination of polyelectrolyte pKa values using surface-to-air tension measurements. *Colloids Surf., A* **2016**, *488*, 15−19.
(138) Solomons, T. W. G.; Fryhle, C. B. *Organic Chemistry*, 10th ed.; John Wiley & Sons, Inc., 2009.
(139) Liu, Y.; Li, C.; Wang, H.-Y.; Zhang, X.-Z.; Zhuo, R.-X. Synthesis of Thermo- and pH-Sensitive Polyion Complex Micelles for Fluorescent Imaging. *Chem. - Eur. J.* **2012**, *18*, 2297−2304.
(140) Rathee, V. S.; Sidky, H.; Sikora, B. J.; Whitmer, J. K. Role of associative charging in the entropy-energy balance of polyelectrolyte complexes. *J. Am. Chem. Soc.* **2018**, *140*, 15319−15328.
(141) Salehi, A.; Larson, R. G. A Molecular Thermodynamic Model of Complexation in Mixtures of Oppositely Charged Polyelectrolytes with Explicit Account of Charge Association/Dissociation. *Macromolecules* **2016**, *49*, 9706−9719.
(142) Friedowitz, S.; Salehi, A.; Larson, R. G.; Qin, J. Role of electrostatic correlations in polyelectrolyte charge association. *J. Chem. Phys.* **2018**, *149*, 163335.
(143) Nap, R.; Gong, P.; Szleifer, I. Weak polyelectrolytes tethered to surfaces: Effect of geometry, acid-base equilibrium and electrical permittivity. *J. Polym. Sci., Part B: Polym. Phys.* **2006**, *44*, 2638−2662.
(144) Longo, G. S.; Cruz, M. O. d. l.; Szleifer, I. Non-monotonic swelling of surface grafted hydrogels induced by pH and/or salt concentration. *J. Chem. Phys.* **2014**, *141*, 124909.
(145) Longo, G.; Olvera de la Cruz, M.; Szleifer, I. Molecular theory of weak polyelectrolyte gels: The role of pH and salt concentration. *Macromolecules* **2007**, *44*, 147.
(146) Gong, P.; Wu, T.; Genzer, J.; Szleifer, I. Behavior of surface-anchored poly(acrylic acid) brushes with grafting density gradients on solid substrates: 2. Theory. *Macromolecules* **2007**, *40*, 8765.
(147) Prusty, D.; Nap, R.; Szleifer, I.; Olvera de la Cruz, M. Charge regulation mechanism in end-tethered weak polyampholytes. *Soft Matter* **2020**, *16*, 8832.
(148) Lytle, T. K.; Sing, C. E. Transfer matrix theory of polymer complex coacervation. *Soft Matter* **2017**, *13*, 7001−7012.
(149) Lytle, T. K.; Sing, C. E. Tuning chain interaction entropy in complex coacervation using polymer stiffness, architecture, and salt valency. *Mol. Syst. Des. Eng.* **2018**, *3*, 183−196.
(150) Madinya, J. J.; Chang, L.-W.; Perry, S. L.; Sing, C. E. Sequence-dependent self-coacervation in high charge-density polyampholytes. *Mol. Syst. Des. Eng.* **2020**, *5*, 632.
(151) Ghasemi, M.; Friedowitz, S.; Larson, R. Analysis of partitioning of salt through doping of polyelectrolyte complex coacervates. *Macromolecules* **2020**, *53*, 6928−6945.
(152) Ong, G. M. C.; Sing, C. E. Mapping the phase behavior of coacervate-driven self-assembly in diblock copolyelectrolytes. *Soft Matter* **2019**, *15*, 5116−5127.
(153) Choi, J.; Rubner, M. F. Influence of the Degree of Ionization on Weak Polyelectrolyte Multilayer Assembly. *Macromolecules* **2005**, *38*, 116−124.
(154) Liu, Y.; Santa Chalarca, C.; Carmean, R.; Olson, R.; Madinya, J.; Sumerlin, B.; Sing, C.; Emrick, T.; Perry, S. Effect of polymer chemistry on the linear viscoelasticity of complex coacervates. *Macromolecules* **2020**, *53*, 7851−7864.
(155) Petrov, A. I.; Antipov, A. A.; Sukhorukov, G. B. Base-acid Equilibria in Polyelectrolyte Systems: From Weak Polyelectrolytes to Interpolyelectrolyte Complexes and Multilayered Polyelectrolyte Shells. *Macromolecules* **2003**, *36*, 10079−10086.
(156) Lou, J.; Friedowitz, S.; Qin, J.; Xia, Y. Tunable coacervation of well-defined homologous polyanions and polycations by local polarity. *ACS Cent. Sci.* **2019**, *5*, 549−557.
(157) Krogstad, D. V.; Lynd, N. A.; Choi, S.-H.; Spruell, J. M.; Hawker, C. J.; Kramer, E. J.; Tirrell, M. V. Effects of polymer and salt concentration on the structure and properties of triblock copolymer coacervate hydrogels. *Macromolecules* **2013**, *46*, 1512−1518.
(158) Lytle, T. K.; Radhakrishna, M.; Sing, C. E. High Charge Density Coacervate Assembly via Hybrid Monte Carlo Single Chain in Mean Field Theory. *Macromolecules* **2016**, *49*, 9693−9705.
(159) Priftis, D.; Xia, X.; Margossian, K. O.; Perry, S. L.; Leon, L.; Qin, J.; de Pablo, J. J.; Tirrell, M. Ternary, tunable polyelectrolyte complex fluids driven by complex coacervation. *Macromolecules* **2014**, *47*, 3076−3085.
(160) Rathee, V.; Sidky, H.; Sikora, B.; Whitmer, J. Explicit Ion Effects on the Charge and Conformation of Weak Polyelectrolytes. *Polymers* **2019**, *11*, 183.

https://doi.org/10.1021/acs.jpcb.1c03065
J. Phys. Chem. B 2021, 125, 8965−8980